

The two-pion spectra for the reaction $\pi^-p \rightarrow \pi^0\pi^0n$ at 38 GeV/c pion momentum and combined analysis of the GAMS, Crystal Barrel and BNL data

V. V. Anisovich*, A. A. Kondashov†, Yu. D. Prokoshkin, S. A. Sadovsky‡, A. V. Sarantsev§
St. Petersburg Nuclear Physics Institute, Gatchina, 188350, Russia
Institute of High Energy Physics, Protvino, Moscow district, 142284, Russia
(May 26, 2021)

We perform the K-matrix analysis of meson partial waves with $IJ^{PC} = 00^{++}, 10^{++}, 02^{++}, 12^{++}$ basing on GAMS data on $\pi^-p \rightarrow \pi^0\pi^0n, \eta\eta n, \eta\eta'n$ together with BNL data on $\pi^-p \rightarrow K\bar{K}n$ and Crystal Barrel data on $p\bar{p}(at\ rest) \rightarrow \pi^0\pi^0\pi^0, \pi^0\eta\eta, \pi^0\pi^0\eta$. The positions of the amplitude poles (physical resonances) are determined as well as the positions of the K-matrix poles (bare states) and the values of bare state couplings to two-meson channels. Nonet classification of the determined bare states is discussed.

12.40.Kj, 13.75.Lb, 14.40.Cs, 14.80.Pb

arXiv:hep-ph/9711319v1 13 Nov 1997

*Electronic address: anisovic@thd.pnpi.spb.ru

†Electronic address: kondashov@mx.ihep.su

‡Electronic address: sadovsky@mx.ihep.su

§Electronic address: vsv@hep486.pnpi.spb.ru

I. INTRODUCTION

With this paper we complete the K-matrix analysis of GAMS data on the reactions $\pi^- p \rightarrow \pi^0 \pi^0 n$ [1], $\eta \eta n$ [2], $\eta \eta' n$ [3] which was started by the papers [4–6]. The K-matrix analysis gives a rich information about meson states, thus helping the $q\bar{q}$ state classification and the search for exotic mesons. However for the restoration of the K-matrix amplitude, one needs to study a full set of open channels with sufficiently high statistics. It is the reason to include in our fit the data on $\pi^- p \rightarrow K\bar{K}n$ [7] and $p\bar{p}(at\ rest) \rightarrow \pi^0 \pi^0 \pi^0$, $\pi^0 \eta \eta$, $\pi^0 \pi^0 \eta$ [8].

K-matrix poles which are a subject of the present consideration differ from the amplitude poles in two points:

(i) The states corresponding to the K-matrix poles do not contain components with real mesons which are inherent in resonances. The absence of a cloud of real mesons allows one to refer conventionally to these states as the bare ones [5,6].

(ii) Due to the transition *bare state* \rightarrow *real mesons* \rightarrow *bare state*, the observed resonances are mixtures of the bare states. So, for the quark systematics, the bare states are primary objects rather than resonances.

Coupling constants *bare state* \rightarrow *real mesons* are responsible not only for the mixing of states but for the resonance decays as well; the relations between couplings allow one to restore the quark/gluon content of bare states [9,10].

The paper is organized as follows.

In Sec. II we introduce a set of formulae which are used in the data fit. We present the S- and D-wave K-matrix amplitudes for the mass-on-shell reactions $\pi\pi \rightarrow \pi\pi, K\bar{K}, \eta\eta, \eta\eta'$ together with those for the mass-off-shell pion in the initial state: $\pi\pi(t)$ with $t \neq m_\pi^2$. The K-matrix formulae for the final state interaction in the three-meson production process, $p\bar{p} \rightarrow$ *three mesons*, are presented as well.

In Sec. III we write down the couplings for the transition *bare state* \rightarrow *two pseudoscalars*, with the imposed quark-combinatorics constraints both for $q\bar{q}$ -states (isoscalar and isovector) and for the glueball. Restoration of couplings in the fit allows us to determine the quark content of isoscalar states and to find a candidate for the glueball.

Mesons which belong to the same $q\bar{q}$ nonet have approximately equal masses; they also have approximately equal decay couplings. Besides, flavour wave functions for isoscalars of the same nonet are orthogonal. In Sec. IV we present the results of the fit with the imposed nonet-classification constraints. Fit of the 00^{++} wave confirms the result of Ref. [6], while for the 02^{++} , 10^{++} , 12^{++} waves the K-matrix representation of amplitudes in the mass region below 1900 MeV is done for the first time. The restored bare states, together with those found in the $K\pi$ S-wave K-matrix analysis [11], allow us to construct the $1^3P_0 q\bar{q}$ and $1^3P_2 q\bar{q}$ nonets unambiguously, and for the $2^3P_0 q\bar{q}$ nonet two variants are possible which dif-

fer in the mass of the lightest scalar/isoscalar state.

The origin of the lightest scalars, $f_0(980)$ and $a_0(980)$, is crucial for the nonet classification. These states are located near the $K\bar{K}$ threshold and give rise to the question whether these states are hadronic $K\bar{K}$ molecules. In Sec. 5 we present arguments based on the direct GAMS measurements together with the results of the performed K-matrix fit that the bare states from which $f_0(980)$ and $a_0(980)$ originate have $q\bar{q}$ nature.

Short summary is given in Sec. 6.

II. EXPERIMENTAL DATA AND K-MATRIX AMPLITUDE

Here we briefly introduce the fitted data and set out the K-matrix formulae used for the data analysis.

A. Experimental data

Simultaneous analysis of meson spectra in the channels $IJ^{PC} = 00^{++}, 10^{++}, 02^{++}$ and 12^{++} is performed on the basis of the following data set:

- (1) GAMS data on the S-wave two-meson production in the reactions $\pi p \rightarrow \pi^0 \pi^0 n$, $\eta \eta n$ and $\eta \eta' n$ at small nucleon momenta transferred, $|t| < 0.2$ (GeV/c)² [1–3];
- (2) GAMS data on the $\pi\pi$ S-wave production in the reaction $\pi p \rightarrow \pi^0 \pi^0 n$ at large momenta transferred, $0.30 < |t| < 1.0$ (GeV/c)² [1];
- (3) GAMS data on the $\pi\pi$ D-wave production in the reaction $\pi p \rightarrow \pi^0 \pi^0 n$, at small and large $|t|$, $0 < |t| < 0.5$ (GeV/c)² [3];
- (4) BNL data on $\pi N \rightarrow K\bar{K}N$ [7];
- (5) Crystal Barrel data on $p\bar{p}(at\ rest) \rightarrow \pi^0 \pi^0 \pi^0$, $\pi^0 \pi^0 \eta$, $\pi^0 \eta \eta$ [8];

B. K-matrix amplitude and analyticity

The K-matrix technique is used for the description of the two-meson coupled channels:

$$A = K(I - i\hat{\rho}K)^{-1}, \quad (1)$$

where K is $n \times n$ matrix, where n is the number of channels under consideration and I is unit matrix. The phase space matrix is diagonal: $\hat{\rho}_{ab} = \delta_{ab}\rho_a$. The phase space factor ρ_a is responsible for the threshold singularities of the amplitude: to keep the amplitude analytic in the physical region under consideration we use analytic continuation for ρ_a below threshold. For example, the $\eta\eta$ phase space factor $\rho_a = (1 - 4m_\eta^2/s)^{1/2}$ is equal to $i(4m_\eta^2/s - 1)^{1/2}$ below the $\eta\eta$ threshold (s is two-meson invariant energy squared). The phase space factors we use lead to false kinematic singularities at $s = 0$ (in all

factors) and at $s = (m_{\eta'} - m_\eta)^2$ (in the $\eta\eta'$ space factor), but these false singularities which are standard for the K-matrix approach are rather distant from the investigated physical region.

For the multimeson phase volume in the isoscalar sector, we use the four-pion phase space defined as either $\rho\rho$ or $\sigma\sigma$ phase space, where σ denotes the S-wave $\pi\pi$ amplitude below 1.2 GeV. The result does not practically depend on whether we use $\rho\rho$ or $\sigma\sigma$ state for the description of multimeson channel: below we provide the formulae and the values of the obtained parameters for the $\rho\rho$ case, for which the fitted expressions are less cumbersome. The multimeson phase space in the sector $I = 1$ is taken in the form which, in its low-energy part, simulates the $a_0\rho$ phase space.

C. Isoscalar/scalar, 00^{++} , partial wave

For the S-wave interaction in the isoscalar sector, we use the parametrization similar to that of Ref. [6]:

$$K_{ab}^{00}(s) = \left(\sum_{\alpha} \frac{g_a^{(\alpha)} g_b^{(\alpha)}}{M_{\alpha}^2 - s} + f_{ab} \frac{1 \text{ GeV}^2 + s_0}{s + s_0} \right) \frac{s - m_{\pi}^2/2}{s}, \quad (2)$$

where K_{ab}^{IJ} is a 5×5 matrix ($a, b = 1, 2, 3, 4, 5$), with the following notations for meson states: 1 = $\pi\pi$, 2 = $K\bar{K}$, 3 = $\eta\eta$, 4 = $\eta\eta'$ and 5 = *multimeson states* (four-pion state mainly at $\sqrt{s} < 1.6$ GeV). The $g_a^{(\alpha)}$ is a coupling constant of the bare state α to the meson channel; the parameters f_{ab} and s_0 describe the smooth part of the K-matrix elements ($s_0 > 1.5$ GeV²). We use the factor $(s - m_{\pi}^2/2)/s$ to suppress the influence of the false kinematic singularity at $s = 0$ in the amplitude near the $\pi\pi$ threshold.

The phase space matrix elements are equal to:

$$\rho_a(s) = \sqrt{\frac{s - 4m_a^2}{s}}, \quad a = 1, 2, 3, \quad (3)$$

where $m_1 = m_{\pi}$, $m_2 = m_K$, $m_3 = m_{\eta}$, and

$$\rho_4(s) = \begin{cases} \rho_{41} & \text{at } s > (m_{\eta} - m_{\eta'})^2 \\ \rho_{42} & \text{at } s < (m_{\eta} - m_{\eta'})^2 \end{cases},$$

$$\rho_{41} = \sqrt{\left(1 - \frac{(m_{\eta} + m_{\eta'})^2}{s}\right) \left(1 - \frac{(m_{\eta} - m_{\eta'})^2}{s}\right)},$$

$$\rho_{42} = 0. \quad (4)$$

The multimeson phase space factor is defined as

$$\rho_5(s) = \begin{cases} \rho_{51} & \text{at } s < 1 \text{ GeV}^2 \\ \rho_{52} & \text{at } s > 1 \text{ GeV}^2 \end{cases},$$

$$\rho_{51} = \rho_0 \int \frac{ds_1}{\pi} \int \frac{ds_2}{\pi} \times M^2 \Gamma(s_1) \Gamma(s_2) \sqrt{(s + s_1 - s_2)^2 - 4s s_1} \times s^{-1} [(M^2 - s_1)^2 + M^2 \Gamma^2(s_1)]^{-1} \times [(M^2 - s_2)^2 + M^2 \Gamma^2(s_2)]^{-1},$$

$$\rho_{52} = 1. \quad (5)$$

Here s_1 and s_2 are the two-pion energies squared, M is ρ -meson mass and $\Gamma(s)$ is its energy-dependent width, $\Gamma(s) = \gamma \rho_1^3(s)$. The factor ρ_0 provides the continuity of $\rho_5(s)$ at $s = 1$ GeV².

The following formulae describe $\pi\pi$, $\eta\eta$ and $\eta\eta'$ production amplitudes due to pion t -channel exchange:

$$A_{\pi N \rightarrow N b} = N (\bar{\Psi}_N \gamma_5 \Psi_N) F_N(t) D(t) \tilde{K}_{\pi\pi(t), a} \times (1 - i\rho K)_{ab}^{-1}, \quad b = \pi\pi, \eta\eta, \eta\eta',$$

$$\tilde{K}_{\pi\pi(t), a} = \left(\sum_{\alpha} \frac{\tilde{g}^{(\alpha)}(t) g_a^{(\alpha)}}{M_{\alpha}^2 - s} + \tilde{f}_a(t) \frac{1 \text{ GeV}^2 + s_0}{s + s_0} \right) \times (s - m_{\pi}^2/2) / s. \quad (6)$$

Here N is a normalization factor, $F_N(t)$ is the nucleon form factor, and $D(t)$ is the pion propagator:

$$F_N(t) = \left[\frac{\tilde{\Lambda} - m_{\pi}^2}{\tilde{\Lambda} - t} \right]^4,$$

$$D(t) = (m_{\pi}^2 - t)^{-1},$$

$$\tilde{g}^{(\alpha)}(t) = g_1^{(\alpha)} + \left(1 - \frac{t}{m_{\pi}^2}\right) (\Lambda_g - \frac{t}{m_{\pi}^2}) g'^{(\alpha)},$$

$$\tilde{f}_a(t) = f_{1a} + \left(1 - \frac{t}{m_{\pi}^2}\right) (\Lambda_f - \frac{t}{m_{\pi}^2}) f'_a, \quad (7)$$

where Λ 's, g' and f' are the fitted parameters.

D. Isoscalar/tensor, 02^{++} , partial wave

The D-wave interaction in the isoscalar sector is parametrized by the 4×4 K-matrix where 1 = $\pi\pi$, 2 = $K\bar{K}$, 3 = $\eta\eta$ and 4 = *multimeson states*:

$$K_{ab}^{0,2}(s) = D_a(s) \left(\sum_{\alpha} \frac{g_a^{(\alpha)} g_b^{(\alpha)}}{M_{\alpha}^2 - s} + f_{ab} \frac{1 \text{ GeV}^2 + s_2}{s + s_2} \right) D_b(s). \quad (8)$$

Factor $D_a(s)$ stands for the D-wave centrifugal barrier. We take this factor in the following form:

$$D_a(s) = \frac{k_a^2}{k_a^2 + 3/r_a^2}, \quad a = 1, 2, \quad (9)$$

where $k_a = \sqrt{s/4 - m_a^2}$ is the momentum of the decaying meson in the c.m. frame of the resonance. For the multimeson decay, the factor $D_5(s)$ is taken to be equal to 1. The phase space factors used are the same as those for the isoscalar S-wave channel.

E. Isovector/scalar, 10^{++} , and isovector/tensor, 12^{++} , partial waves

For the amplitude in the isovector/scalar and isovector/tensor channels, we use the 4×4 K-matrix with $1 = \pi\eta$, $2 = K\bar{K}$, $3 = \pi\eta'$ and $4 = \text{multimeson states}$:

$$K_{ab}^{1J}(s) = D_a(s) \left(\sum_{\alpha} \frac{g_a^{(\alpha)} g_b^{(\alpha)}}{M_{\alpha}^2 - s} + f_{ab} \frac{1.5 \text{ GeV}^2 + s_1}{s + s_1} \right) D_b(s). \quad (10)$$

Here $J = 0, 2$; the factors $D_a(s)$ are equal to 1 for the 10^{++} amplitude, while for the D-wave partial amplitude the factor $D_a(s)$ is taken in the form:

$$D_a(s) = \frac{k_a^2}{k_a^2 + 3/r_3^2}, \quad a = 1, 2, 3, \\ D_4(s) = 1. \quad (11)$$

The elements of the phase space matrix in the isovector sector are defined as

$$\rho_1(s) = \begin{cases} \rho_{11} & \text{at } s > (m_{\eta} - m_{\pi})^2 \\ \rho_{12} & \text{at } s < (m_{\eta} - m_{\pi})^2 \end{cases},$$

$$\rho_{11} = \sqrt{\left(1 - \frac{(m_{\eta} + m_{\pi})^2}{s}\right) \left(1 - \frac{(m_{\eta} - m_{\pi})^2}{s}\right)}, \\ \rho_{12} = 0, \quad (12)$$

$$\rho_2(s) = \sqrt{\frac{s - 4m_K^2}{s}}, \quad (13)$$

$$\rho_3(s) = \begin{cases} \rho_{31} & \text{at } s > (m'_{\eta} - m_{\pi})^2 \\ \rho_{32} & \text{at } s < (m'_{\eta} - m_{\pi})^2 \end{cases},$$

$$\rho_{31} = \sqrt{\left(1 - \frac{(m'_{\eta} + m_{\pi})^2}{s}\right) \left(1 - \frac{(m'_{\eta} - m_{\pi})^2}{s}\right)}, \\ \rho_{32} = 0. \quad (14)$$

The multimeson phase space factor $\rho_4(s)$ is taken in the form which simulates the ρ_{a0} phase space factor below $s = 2.25 \text{ GeV}^2$:

$$\rho_4(s) = \begin{cases} \rho_{41} & \text{at } (m_{\eta} + 3m_{\pi})^2 < s < 2.25 \text{ GeV}^2 \\ \rho_{42} & \text{at } s > 2.25 \text{ GeV}^2 \\ \rho_{43} & \text{at } s < (m_{\eta} + 3m_{\pi})^2 \end{cases}, \\ \rho_{41} = \left(\frac{1 - (m_{\eta} + 3m_{\pi})^2/s}{1 - (m_{\eta} + 3m_{\pi})^2/2.25 \text{ GeV}^2} \right)^{5/2}, \\ \rho_{42} = 1, \\ \rho_{43} = 0. \quad (15)$$

F. Three-meson production amplitudes

The amplitudes $p\bar{p}$ (*at rest*) $\rightarrow \pi^0\pi^0\pi^0$, $\pi^0\eta\eta$ which correspond to the production of the two-meson isoscalar states are equal to:

$$A_{p\bar{p} \rightarrow \text{three mesons}} = A_1(23) + A_2(13) + A_3(12),$$

where the amplitude $A_k(s_{ij})$ stands for diagrams with an interaction of particles in the intermediate states and the last interaction being of the particles i and j , while the particle k is a spectator. We suppose, as in the previous papers [5,6], that $p\bar{p}$ annihilates at rest from the 1S_0 -level. The following form is used for the two-particle interaction block:

$$A_1(23) = \sum_{J=0,2} X_J(23) \tilde{K}_{p\bar{p}\pi,a}^{0J}(s_{23}) \\ \times (1 - i\hat{\rho}K^{0J}(s_{23}))_{ab}^{-1}. \quad (16)$$

Here $b = \pi^0\pi^0$ stands for $\pi^0\pi^0\pi^0$ production, and $b = \eta\eta$ for $\pi^0\eta\eta$. The centrifugal barrier factor X_J is equal to 1 for the production of the S-wave resonance. For the D-wave resonance production, this factor is:

$$X_2(23) = \frac{1}{2}(3 \cos^2 \Theta_{12} - 1) \frac{p_1^2}{p_1^2 + 3/R^2}, \quad (17)$$

where Θ_{12} is the angle between particles 1 and 2 in the rest frame of the particles 2 and 3, p_1 is the momentum of the particle 1 in this frame and R characterizes the annihilation radius. The \tilde{K} -matrices which describe the prompt resonance production in the $p\bar{p}$ annihilation have the following form:

$$\tilde{K}_{p\bar{p}\pi,a}^{00}(s_{ij}) = \left(\sum_{\alpha} \frac{\Lambda_{p\bar{p}\pi}^{(\alpha)}[00]g_{\alpha}^{(\alpha)}}{M_{\alpha}^2 - s_{ij}} + \phi_{p\bar{p}\pi,a}[00] \right. \\ \left. \times \frac{1 \text{ GeV}^2 + s_0}{s_{ij} + s_0} \right) \left(\frac{s_{ij} - m_{\pi}^2/2}{s_{ij}} \right), \quad (18)$$

$$\tilde{K}_{p\bar{p}\pi,a}^{02}(s_{ij}) = \left(\sum_{\alpha} \frac{\Lambda_{p\bar{p}\pi}^{(\alpha)}[02]g_{\alpha}^{(\alpha)}}{M_{\alpha}^2 - s_{ij}} + \phi_{p\bar{p}\pi,a}[0,2] \right. \\ \left. \times \frac{1 \text{ GeV}^2 + s_0}{s_{ij} + s_0} \right) D_a(s_{ij}). \quad (19)$$

The $\pi\pi\pi$ production amplitude is completely described by eqs. (16)-(19) because of the amplitude symmetry under the rotation of pion indices i, j, k .

The part of the amplitude $p\bar{p}$ (*at rest*) $\rightarrow \pi\pi^0\pi^0$, which corresponds to the production of isoscalar resonances, reads:

$$A_1(23) = \sum_{J=0,2} X_J(23) \tilde{K}_{p\bar{p}\pi,a}^{0J}(s_{23}) \\ (1 - i\rho K^{0J}(s_{23}))_{ab}^{-1}, \quad b = \pi^0\pi^0, \quad (20)$$

where

$$\tilde{K}_{p\bar{p}\eta,a}^{00}(s_{ij}) = \left(\sum_{\alpha} \frac{\Lambda_{p\bar{p}\eta}^{(\alpha)}[00]g_a^{(\alpha)}}{M_{\alpha}^2 - s_{ij}} + \phi_{p\bar{p}\eta,a}[00] \times \frac{1 \text{ GeV}^2 + s_0}{s_{ij} + s_0} \right) \left(\frac{s_{ij} - m_{\pi}^2/2}{s_{ij}} \right). \quad (21)$$

Parameters $\Lambda_{p\bar{p}\pi}^{\alpha}[0J]$ and $\phi_{p\bar{p}\pi}[0J]$ (or $\Lambda_{p\bar{p}\eta}^{\alpha}[0J]$ and $\phi_{p\bar{p}\eta}[0J]$) may be complex magnitudes with different phases due to the three particle interactions.

The part of the amplitude, which corresponds to the production of the isovector resonances in the reaction $p\bar{p}$ (*at rest*) $\rightarrow \eta\eta\pi^0$, is written as $A_1(23) + A_2(13)$ and

$$A_2(13) = \sum_{J=0,2} X_J(13) \tilde{K}_{p\bar{p}\eta,a}^{1J}(s_{13}) \times (1 - i\hat{\rho}K^{1J}(s_{13}))_{ab}^{-1}, \quad b = \eta\pi^0, \quad (22)$$

where

$$\tilde{K}_{p\bar{p}\eta,a}^{1J}(s_{ij}) = \left(\sum_{\alpha} \frac{\Lambda_{p\bar{p}\eta}^{(\alpha)}[1J]g_a^{(\alpha)}}{M_{\alpha}^2 - s_{ij}} + \phi_{p\bar{p}\eta,a}[1J] \frac{1 \text{ GeV}^2 + s_1}{s_{ij} + s_1} \right) D_a(s_{ij}). \quad (23)$$

The production of isovector resonances in the reaction $p\bar{p}$ (*at rest*) $\rightarrow \pi^0\pi^0\eta$ has the form $A_1(23) + A_2(13)$ and

$$A_2(13) = \sum_{J=0,1,2} X_J(13) \tilde{K}_{p\bar{p}\pi,a}^{1J}(s_{13}) \times (1 - i\hat{\rho}K^{1J}(s_{13}))_{ab}^{-1}, \quad b = \eta\pi^0, \quad (24)$$

where $\tilde{K}_{p\bar{p}\pi,a}^{1J}$ is given by Eq. (23) with the replacement $\Lambda_{p\bar{p}\eta}^{(\alpha)}[1J] \rightarrow \Lambda_{p\bar{p}\pi}^{(\alpha)}[1J]$ and $\phi_{p\bar{p}\eta,a}[1J] \rightarrow \phi_{p\bar{p}\pi,a}[1J]$.

III. QUARK-COMBINATORIC RULES FOR THE DECAY COUPLINGS AND THE $q\bar{q}$ CONTENT OF MESONS

The decay couplings of the $q\bar{q}$ -meson and glueball to the two mesons are determined by the diagrams with $q\bar{q}$ -pairs produced by gluons. Figs. 1(b),(c) provide an example of diagrams which contribute to the leading terms in the $1/N$ expansion [12] and Fig. 1(d) is an example of diagrams for the next-to-leading contribution. The production of soft $q\bar{q}$ pairs by gluons violates flavour symmetry, with the following ratios of the production probabilities:

$$u\bar{u} : d\bar{d} : s\bar{s} = 1 : 1 : \lambda, \quad (25)$$

and $\lambda = 0.4 - 0.8$ [13]. In our fit we fix $\lambda = 0.6$.

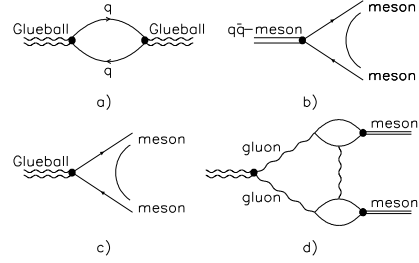


FIG. 1. Quark-antiquark loop diagram which determines the glueball width (a); diagrams for the decay of a $q\bar{q}$ -meson (b) and a glueball (c),(d) into two $q\bar{q}$ -meson states.

We calculate the ratios of the decay coupling constants in the framework of the quark combinatoric rules which were previously suggested for the high energy hadron production [14] and then extended for hadronic J/Ψ decays [15]. Calculations of the decay coupling constants for the glueball and isoscalar/scalar $q\bar{q}$ -mesons were performed in Refs. [5,9,10]. The decay couplings for isoscalar and isovector mesons are given in Tables I and II.

Isoscalar meson decay couplings depend on the non-strange/strange component ratio of the decaying meson given by the mixing angle Φ :

$$\psi_{\text{decaying meson}}^{\text{flavour}} = n\bar{n}C\cos\Phi + s\bar{s}S\sin\Phi. \quad (26)$$

Here $n\bar{n} = (u\bar{u} + d\bar{d})/\sqrt{2}$. It allows us to restore Φ and at the same time to determine the decay couplings.

The glueball decay couplings obey the same ratios as the isoscalar/scalar $q\bar{q}$ -meson couplings with the mixing angle equal to:

$$\Phi = \Phi_{\text{glueball}}, \quad \tan\Phi_{\text{glueball}} = \sqrt{\lambda/2}. \quad (27)$$

It follows from the two-stage decay of the glueball [10], see Fig. 1(c): an intermediate $q\bar{q}$ -state in the glueball decay is a mixture of $n\bar{n}$ and $s\bar{s}$ quarks produced in proportion given by Eq. (25). We fix $\Phi_{\text{glueball}} = 25^\circ \pm 5^\circ$.

The coincidence of the glueball decay couplings with those of $q\bar{q}$ meson at $\Phi = \Phi_{\text{glueball}}$ points out that there is no simple signature of a determination of glueball state: searching for the glueball, we should perform a full $q\bar{q}$ -classification of mesons, thus an existence of an extra state for the $q\bar{q}$ -classification is an indication of the exotics.

The normalization in Table I is done in such a way that for the glueball decay the summation of couplings squared over all channels is proportional to the probability to produce a two-quark pair, $(2 + \lambda)^2$, see Eq. (25). So,

$$\begin{aligned}\sum_{\text{channels}} G^2(c)I(c) &= \frac{1}{2}G^2(2+\lambda)^2, \\ \sum_{\text{channels}} g_G^2(c)I(c) &= \frac{1}{2}g_G^2(2+\lambda)^2.\end{aligned}\quad (28)$$

Here $I(c)$ is the identity factor and $c = \pi^0\pi^0$, $\pi^+\pi^-$, K^+K^- , and so on (see Table I). With this normalization $g_G/G \simeq 1/N_c$. The experience of the quark-gluon diagram calculations teaches us that the factor $1/N_c$ actually leads to a suppression of the order of $1/10$: in the fitting procedure we impose a restriction $|g_G/G| < 1/3$.

The nonet classification of isoscalar mesons is based on the following two constraints:

- (1) The angle difference between isoscalar nonet partners should be 90° . For this value the corridor $\pm 5^\circ$ is allowed in our analysis:

$$\Phi(1) - \Phi(2) = 90^\circ \pm 5^\circ. \quad (29)$$

- (2) Coupling constants g of Tables I and II should be approximately equal to each other for all nonet partners:

$$g[f_J(1)] \simeq g[f_J(2)] \simeq g[a_J] \simeq g[K_J]. \quad (30)$$

The conventional quark model requires exact coincidence of the couplings g but the energy dependence of the loop diagram of Fig. 1(a), $B(s)$, may violate this coupling constant equality because of the mass splitting inside a nonet. The K-matrix coupling constant contains an additional s -dependent factor as compared to the coupling of the N/D-amplitude [10]: $g^2(K) = g^2(N/D)/(1+B'(s))$. The factor $(1+B'(s))^{-1}$ mostly affects the low- s region due to the threshold and left-hand side singularities of the partial amplitude. Therefore, the coupling constant equality is mostly violated for the lightest 00^{++} nonet, $1^3P_0 q\bar{q}$. We allow for the members of this nonet $1 \leq g[f_0(1)]/g[f_0(2)] \leq 1.5$. For the $2^3P_0 q\bar{q}$ nonet members, we put the two-meson couplings equal both for isoscalar and isovector mesons. The equality of coupling constants is also imposed for tensor resonances.

IV. DESCRIPTION OF DATA AND THE RESULTS

The performed K-matrix fit gives a good description of the data, see Figs. 2-6. The χ^2 values for the fit are shown in Table III and parameters of the fit are presented in Tables IV-VII. Below we single out the main results of our fit.

A. $IJ^{PC} = 00^{++}$ wave

The present fit confirms the results obtained in the previous analysis of the 00^{++} wave [4–6]. For the description

of the 00^{++} wave in the mass region below 2000 MeV, five K-matrix poles are needed (a four-pole amplitude fails to describe well the data set under consideration). Correspondingly, five bare states are found:

$$\begin{aligned}f_0^{\text{bare}}(720 \pm 100), \\ \psi^{\text{flavour}} &= (0.45 \pm 0.1)n\bar{n} - (0.89 \pm 0.05)s\bar{s}, \\ f_0^{\text{bare}}(1230 \pm 50), \\ \psi^{\text{flavour}} &= (0.9^{+0.05}_{-0.2})n\bar{n} + (0.45^{+0.3}_{-0.1})s\bar{s}, \\ f_0^{\text{bare}}(1260 \pm 30), \\ \psi^{\text{flavour}} &= (0.93^{+0.02}_{-0.1})n\bar{n} + (0.37^{+0.2}_{-0.06})s\bar{s}, \\ f_0^{\text{bare}}(1600 \pm 50), \\ \psi^{\text{flavour}} &= (0.95 \pm 0.05)n\bar{n} + (0.3^{+0.14}_{-0.4})s\bar{s}, \\ f_0^{\text{bare}}(1810 \pm 30), \\ \psi^{\text{flavour}} &= \begin{cases} (0.10 \pm 0.05)n\bar{n} + (0.995^{+0.005}_{-0.015})s\bar{s}, \\ \text{Solution I),} \\ (0.67 \pm 0.08)n\bar{n} - (0.74 \pm 0.08)s\bar{s}, \\ \text{(Solution II).} \end{cases}\end{aligned}\quad (31)$$

Experimental data used in the fit do not fix unambiguously the flavour wave function of $f_0^{\text{bare}}(1810 \pm 30)$: two solutions are found for it.

The scattering amplitude has five poles in the energy complex plane, four of them correspond to relatively narrow resonances while the fifth resonance is very broad:

$$\begin{aligned}f_0(980) &\rightarrow (1015 \pm 15) - i(43 \pm 8) \quad \text{MeV}, \\ f_0(1300) &\rightarrow (1300 \pm 20) - i(120 \pm 20) \quad \text{MeV}, \\ f_0(1500) &\rightarrow (1499 \pm 8) - i(65 \pm 10) \quad \text{MeV}, \\ f_0(1530) &\rightarrow (1530^{+90}_{-250}) - i(560 \pm 140) \quad \text{MeV}, \\ f_0(1780) &\rightarrow \begin{cases} (1780 \pm 30) - i(140 \pm 20) \text{ MeV}, \\ \text{(Solution I),} \\ (1780 \pm 50) - i(220 \pm 50) \text{ MeV}, \\ \text{(Solution II).} \end{cases}\end{aligned}\quad (32)$$

The broad resonance is crucial for the description of the 00^{++} wave, being responsible for large interference effects which are seen in different reactions. Namely, the resonance $f_0(980)$ reveals itself as a dip in the S-wave $\pi\pi \rightarrow \pi\pi$ -spectrum, Fig. 2(a), and as a sharp peak in the $\pi\pi(t) \rightarrow \pi\pi$ spectra at large $|t|$, Fig. 3. The resonance $f_0(1300)$ is seen in the $\pi\pi(t) \rightarrow \pi\pi$ spectra at large $|t|$ as a well shaped bump, Fig. 3, while in the $\pi\pi \rightarrow \pi\pi$ and $\pi\pi \rightarrow K\bar{K}$ spectra it reveals itself as a shoulder, Figs. 2 and 5. $f_0(1500)$ is seen as a dip in the $\pi\pi \rightarrow \pi\pi$ and $\pi\pi \rightarrow \eta\eta$ spectra, Figs. 2, 5, and as a peak in $p\bar{p}(at \text{ rest}) \rightarrow \pi^0\pi^0\pi^0$ reaction, Fig. 6. In all these appearances of $f_0(980)$, $f_0(1300)$ and $f_0(1500)$, their interference with $f_0(1530^{+90}_{-250})$ plays a decisive role. In the case of large interference effects it is useful to display the amplitude on the Argand-plot. The Argand-plots for the amplitudes $\pi\pi \rightarrow \pi\pi$, $\pi\pi \rightarrow \eta\eta$, $\pi\pi \rightarrow K\bar{K}$, $\pi\pi \rightarrow \eta\eta'$ and $\pi\pi(t) \rightarrow \pi\pi$ are shown in Figs. 7 and 8.

Four bare states of Eq. (31) can be naturally classified as nonet partners of the $q\bar{q}$ multiplets 1^3P_0 and 2^3P_0 . The fifth bare state is superfluous for the $q\bar{q}$ classification being a good candidate for the lightest scalar glueball. Eq. (31) gives two variants for the glueball: either it is a bare state with mass near 1250 MeV or it is located near 1600 MeV. Correspondingly, after having imposed the constraints (29) and (30), we found the following variants of the nonet classification. For the solution **I**:

- I.** $f_0^{\text{bare}}(720)$ and $f_0^{\text{bare}}(1260)$ are 1^3P_0 nonet partners,
 $f_0^{\text{bare}}(1600)$ and $f_0^{\text{bare}}(1810)$ are 2^3P_0 nonet partners,
 $f_0^{\text{bare}}(1230)$ is a glueball.

Within solution **II**, two variants describe well the data set:

- II-1.** $f_0^{\text{bare}}(720)$ and $f_0^{\text{bare}}(1260)$ are 1^3P_0 nonet partners,
 $f_0^{\text{bare}}(1600)$ and $f_0^{\text{bare}}(1810)$ are 2^3P_0 nonet partners,
 $f_0^{\text{bare}}(1230)$ is a glueball;

- II-2.** $f_0^{\text{bare}}(720)$ and $f_0^{\text{bare}}(1260)$ are 1^3P_0 nonet partners,
 $f_0^{\text{bare}}(1230)$ and $f_0^{\text{bare}}(1810)$ are 2^3P_0 nonet partners,
 $f_0^{\text{bare}}(1600)$ is a glueball.

Tables IV-V present parameters which correspond to these three variants.

Lattice calculations of the gluodynamic glueball [16] give the mass of the lightest scalar state in the region 1550-1750 MeV that coincides with the variant **II-2**. However, it should be emphasized that the state $f_0^{\text{bare}}(1600)$ can not be identified as a pure gluodynamic glueball because f_0^{bare} 's contain the $q\bar{q}$ -components related to real parts of the loop transition diagrams: this problem is discussed in detail in Refs. [10,17,18]. An extraction of the $q\bar{q}$ -component from $f_0^{\text{bare}}(1600)$ leads to the mass shift of the state which is not large according to Refs. [10,18]: $f_0^{\text{bare}}(1600) \rightarrow f_0^{\text{pure glueball}}(1633)$.

B. $IJ^{PC} = 10^{++}$ wave

Two isovector/scalar resonances are well seen in the $p\bar{p}$ annihilation into three mesons [5,6,8,19,20]. The lightest one is the well known $a_0(980)$, while the next resonance is the newly discovered $a_0(1450)$ with mass 1450 ± 40 MeV and width $\Gamma = 270 \pm 40$ MeV, as is given by the Particle Data Group [21]. Let us note that in fitting the last high statistic Crystal Barrel data with the T-matrix method used for this wave [6,19,20] the mass of this resonance appeared to be a bit higher and equal to

1520 ± 40 MeV. A similar result is obtained in the present K-matrix approach.

For the description of the isovector/isoscalar scattering amplitude, we use the two-pole 4×4 K-matrix with two-meson coupling constants given in Table II.

In the first stage of the fit, the coupling of the lightest a_0 -state was allowed to vary in the interval bounded by $g[f_0^{\text{bare}}(720)]$ and $g[f_0^{\text{bare}}(1260)]$. In all the variants of the fit, the two-meson coupling constant of the lightest state, $g[a_0^{\text{bare}}(\textit{lightest state})]$, appeared to be very close to the coupling constant $g[f_0^{\text{bare}}(1260)]$: in the final fit, in line with the constraint of Eq. (30), we fix these couplings equal to each other. The two-meson coupling of the next isovector/scalar is fixed to be equal to the couplings of the 2^3P_0 isoscalar/scalar states.

The fit gives two solutions for the 10^{++} wave which practically coincide in terms related to the resonance/bare-state sector and differ in background terms. Parameters for the 10^{++} wave and the pole position are given in Table VI. We have for the resonance positions and the bare states, correspondingly:

$$\begin{aligned} a_0(980) &\rightarrow (988 \pm 6) - i(46 \pm 10) \text{ MeV}, \\ a_0(1450) &\rightarrow (1535 \pm 30) - i(146 \pm 20) \text{ MeV} \end{aligned} \quad (33)$$

and

$$a_0^{\text{bare}}(964 \pm 16), \quad a_0^{\text{bare}}(1670 \pm 80). \quad (34)$$

But these two solutions give different predictions for the scattering amplitudes: for the first solution (without K-matrix background terms) the $\pi\eta \rightarrow \pi\eta$ scattering amplitude squared (see Fig. 9) has a dip in the region of $a_0(1450)$ due to the destructive resonance interference with the background, while for the second solution (with the K-matrix background terms) a dip appears at 1100 MeV. In the present fit, the information on the isovector/scalar wave comes from Crystal Barrel data only. These data being rather sensitive to the pole structure provide poor information about K-matrix background terms: it is a source of ambiguities in our K-matrix solution. But, let us stress, the description of other partial waves practically does not depend on whether the first or second solution is used: the variation of parameters is within the given errors.

C. $IJ^{PC} = 12^{++}$ wave

Similar to the isovector/scalar case, the 4×4 two-pole K-matrix is used for the description of the 12^{++} -wave. Coupling constants of bare states and the poles of the scattering amplitude are given in Table VII. We have determined two bare states:

$$a_2^{\text{bare}}(1314 \pm 7), \quad a_2^{\text{bare}}(1670 \pm 75). \quad (35)$$

The poles of the amplitude are located at

$$\begin{aligned}
a_2(1320) &\rightarrow (1309 \pm 6) - i(58 \pm 6) \text{ MeV}, \\
a_2(1640) &\rightarrow (1640 \pm 50) - i(122 \pm 18) \text{ MeV}
\end{aligned} \tag{36}$$

The lightest state is a well known $a_2(1320)$ resonance, with mass 1318 ± 1 MeV and width $\Gamma = 107 \pm 5$ MeV, according to Ref. [21].

When fitting Crystal Barrel data on the reaction $p\bar{p}(\text{at rest}) \rightarrow \eta\pi\pi$, the introduction of the isovector/tensor resonance with mass 1600-1700 MeV makes an appreciable improvement of the Dalitz plot description in this region.

D. $IJ^{PC} = 02^{++}$ wave

The two lightest isoscalar/tensor states, $f_2(1270)$ and $f_2'(1525)$, are well known: they are members of the nonet $1^3P_2 q\bar{q}$. Crystal Barrel data point out the existence of the resonance $f_2(1565)$ which helps to describe the $p\bar{p} \rightarrow \pi^0\pi^0\pi^0$ Dalitz plot in the region of large two-pion masses [8,17,20]. Because of that, we also begin our analysis introducing a three-pole K-matrix amplitude. However, after imposing the nonet constraints on the 1^3P_2 states, see eqs. (28) and (29), we obtain that the couplings of the third state turn out to be negligibly small. Although the description of the reaction $p\bar{p} \rightarrow \eta\eta\pi^0$ becomes a bit worse under the imposed constraints (about 0.1 per degree of freedom for χ^2), the description of the reaction $p\bar{p} \rightarrow \pi^0\pi^0\pi^0$ (where $f_2(1560)$ is seen according to [8,17,20]) improves χ^2 by 0.07 giving practically the same total χ^2 .

$f_2(1560)$ is not seen in GAMS data; that gives a strong restriction on the partial width of the resonance decay into $\pi\pi$ channel, less than 20 MeV.

In our final fit, we have used the two-pole K-matrix amplitude with the nonet constraints; parameters for this fit are presented in Table VII.

The K-matrix fit gives the following bare isoscalar/tensor states, the members of the 3P_2 nonet:

$$\begin{aligned}
f_2^{\text{bare}}(1235 \pm 10), f_2^{\text{bare}}(1530 \pm 10), \\
\Phi[f_2^{\text{bare}}(1530)] = 86^\circ \pm 5^\circ.
\end{aligned} \tag{37}$$

The K-matrix 02^{++} amplitude has poles at the complex mass values:

$$\begin{aligned}
f_2(1270) &\rightarrow (1262 \pm 6) - i(90 \pm 7) \text{ MeV}, \\
f_2'(1525) &\rightarrow (1518 \pm 9) - i(71 \pm 10) \text{ MeV}.
\end{aligned} \tag{38}$$

These values should be compared with masses and half-widths of Particle Data Group [21] which are, correspondingly: (1275 ± 5) MeV, (92.5 ± 10) MeV and (1525 ± 5) MeV, (38 ± 5) MeV. The width of $f_2'(1525)$ found in our fit appears to be much larger than one given in PDG. It is quite possible that in fitting the present data set we cannot resolve a possible D-wave double pole structure in the region of 1530 MeV caused by

the $f_2'(1525)$ and $f_2(1560)$ resonances, for they are located near the edge of the phase space for Crystal Barrel data, while GAMS data give a restriction only on the couplings to $\pi\pi$ channel. It is possible that the additional information from Crystal Barrel data on $KK\pi$ production together with GAMS [22] and VES data [23] on $\omega\omega$ production will clarify this point.

E. Nonet classification

The results of the performed analysis together with the results of the K-matrix analysis of the $K\pi$ S-wave [11] allow us to construct the lightest scalar $q\bar{q}$ nonet uniquely as

$$\begin{aligned}
1^3P_0 : f_0^{\text{bare}}(720 \pm 100), \\
f_0^{\text{bare}}(1260 \pm 30), \\
a_0^{\text{bare}}(960 \pm 30), \\
K_0^{\text{bare}}(1220_{-150}^{+50}), \\
\Phi[f_0^{\text{bare}}(720)] = -70^\circ_{-16^\circ}^{+5^\circ}.
\end{aligned} \tag{39}$$

The lightest scalar, $f_0^{\text{bare}}(720 \pm 100)$, is dominantly a $s\bar{s}$ state with mixing angle close to the ideal octet one, $\Phi_{\text{ideal octet}} = -55^\circ$. The situation with the lightest scalar nonet is similar to that with the lightest pseudoscalar nonet, where the mixing angle for the η -meson is also close to the $\Phi_{\text{ideal octet}}$: this definitely indicates the degeneration of the lightest 00^{++} and 00^{-+} states.

The multiplet of the lightest tensor states appears as

$$\begin{aligned}
1^3P_2 : f_2^{\text{bare}}(1240 \pm 10), \\
f_2^{\text{bare}}(1522 \pm 10), \\
a_2^{\text{bare}}(1311 \pm 3), \\
K_2^*(1430) \\
\Phi[f_2^{\text{bare}}(1240)] = -10^\circ \pm 3^\circ.
\end{aligned} \tag{40}$$

The K-matrix analysis of the πK D-wave is not done: the $(J=2)\pi K$ resonance with mass 1431 ± 3 is reported in Ref. [24]; we have used this resonance to complete the multiplet (40).

Our analysis gives two variants for the 2^3P_0 $q\bar{q}$ -nonet: First variant:

$$\begin{aligned}
2^3P_0 : f_0^{\text{bare}}(1600 \pm 50), \\
f_0^{\text{bare}}(1810 \pm 30), \\
a_0^{\text{bare}}(1650 \pm 50), \\
K_0^{\text{bare}}(1885_{-100}^{+50}), \\
\Phi[f_0^{\text{bare}}(1810)] = 84^\circ \pm 5^\circ
\end{aligned} \tag{41}$$

The state $K_0^{\text{bare}}(1885_{-150}^{+50})$ is fixed by the analysis [11] of the $K\pi$ S-wave. In this variant the lightest glueball

state is $f_0^{\text{bare}}(1230_{-30}^{+150})$. In the second variant the lightest glueball state is identified as $f_0^{\text{bare}}(1600)$, namely:

$$\begin{aligned}
2^3P_0 : f_0^{\text{bare}}(1230_{-30}^{+150}), \\
f_0^{\text{bare}}(1810 \pm 30), \\
a_0^{\text{bare}}(1650 \pm 50), \\
K_0^{\text{bare}}(1885_{-100}^{+50}), \\
\Phi[f_0^{\text{bare}}(1810)] = 44^\circ \pm 10^\circ
\end{aligned} \tag{42}$$

V. RESONANCES $f_0(980)$ AND $a_0(980)$: ARE THEY $K\bar{K}$ MOLECULES?

First, let us discuss the origin of $f_0(980)$. GAMS data for the $f_0(980)$ production at large $|t|$, see Fig. 3, directly demonstrate that this resonance has a hard component, while the location of the pole near the $K\bar{K}$ threshold definitely says that its kaon component is a long-range one. The existence of the long-range component gives rise to discussion about molecular structure for this state [25]. The problem to discuss is how substantial are these components in the formation of the resonance. Remember that the short-range component (with $r < 1$ fm) is a subject of quark/gluon considerations and quark systematics.

The resonance $f_0(980)$ corresponds to the two poles located at (in MeV units):

$$\begin{aligned}
M &= 1015 - i46 \quad (II \text{ sheet, under } \pi\pi - \text{cut}), \\
M &= 936 - i238 (III \text{ sheet, under } \pi\pi \text{ and } K\bar{K} \text{ cuts}).
\end{aligned}$$

The second pole appears due to well-known double-pole structure caused by the $K\bar{K}$ -threshold (see, for example, [26]), while the first pole at $M = 1015 - i46$ MeV generates the leading irregularities in $\pi\pi$ spectra.

The restored K-matrix amplitude allows one to see the role of the $K\bar{K}$ component in the formation of $f_0(980)$, thus clarifying if this resonance is a descendant of a $q\bar{q}$ state or is a molecular-type system. To this aim, let us switch off the $f_0(980)$ decay processes (transitions into $\pi\pi$ and $K\bar{K}$) and look at the dynamics of pole positions, with gradual onset of couplings. For the gradual change of couplings we performed the replacement in the K-matrix 00^{++} -amplitude:

$$g_a^{(\alpha)} \rightarrow \xi g_a^{(\alpha)}. \tag{43}$$

Parameter ξ varies in the interval:

$$0 < \xi \leq 1. \tag{44}$$

At $\xi \rightarrow 0$ the decay channels are switched off, and we have a bare state, while at $\xi = 1$ the real case is restored.

At $\xi \rightarrow 0$ the masses of the lightest scalar bare states are 650 and 1260 MeV (the positions of the K-matrix

poles). The trajectories of states with increasing ξ are shown in Fig. 10.

The crucial point is what component, $\pi\pi$ or $K\bar{K}$, is mainly responsible for the mass shift from 650 MeV to $1020 - i48$ MeV. We can elucidate this point, switching off the $K\bar{K}$ component and leaving $\pi\pi$ untouched, and vice versa. In the first case the mass of $f_0(980)$ state is:

$$M(\text{without } K\bar{K}) = 974 - i115 \text{ MeV}. \tag{45}$$

One sees that the mass shift

$$\begin{aligned}
\delta_{K\bar{K}} = M(\xi = 1) - M(\text{without } K\bar{K}) = \\
41 + i67 \text{ MeV}
\end{aligned} \tag{46}$$

is not large: the $K\bar{K}$ -component which is responsible for the value of δ does not play an important role in the formation of the mass of $f_0(980)$. In the second case, when the $\pi\pi$ component is switched off, we get the nearest state to the $K\bar{K}$ threshold, which is located at:

$$M(\text{without } \pi\pi) = 810 - i10 \text{ MeV}. \tag{47}$$

So the mass shift is

$$\begin{aligned}
\delta_{\pi\pi} = M(\xi = 1) - M(\text{without } \pi\pi) = \\
205 + i36 \text{ MeV},
\end{aligned} \tag{48}$$

being much larger than $\delta_{K\bar{K}}$. The transition into real pions,

$$f_0^{\text{bare}}(720) \rightarrow \pi\pi \tag{49}$$

is mainly in charge of the mixing of the lightest scalar $q\bar{q}$ state with other scalars thus shifting its mass by chance to the region of the next threshold, $K\bar{K}$. The $K\bar{K}$ component of $f_0(980)$ is of the molecule-type: relative kaon momenta are small, so relative distances are large. But, let us stress again, the two-kaon component does not play a crucial role in the formation of the mass of $f_0(980)$.

VI. CONCLUSION

We have performed the K-matrix analysis of GAMS data on the S- and D-wave $\pi^0\pi^0$, $\eta\eta$ and $\eta\eta'$ data, together with data obtained by BNL and Crystal Barrel Collaboration. Partial amplitudes for the states 00^{++} , 02^{++} , 10^{++} and 12^{++} are investigated in the mass region up to 2000 MeV, the poles of these amplitudes are found, see Tables IV-VII. Pole terms of the K-matrix are restored, i.e. the bare states with quantum numbers 00^{++} , 02^{++} , 10^{++} and 12^{++} are found. The quark content of these bare states is determined, based on the relations between coupling constants of the decays: this allows to restore the quark nonets 1^3P_0 , 2^3P_0 and 1^3P_2 . The performed analysis confirms the result of Ref. [6] which is based on the K-matrix analysis of the 00^{++} wave only: in the region 1200-1600 MeV there exists a scalar/isoscalar

state which is superfluous for the $q\bar{q}$ systematics. This state is a good candidate for the lightest scalar glueball.

The analysis indicates the degeneration of the lightest 00^{++} and 00^{-+} states.

Acknowledgements

We thank D. V. Bugg, S. S. Gershtein, A. K. Likhoded, L. Montanet and B. S. Zou for useful discussions and Crystal Barrel Collaboration for providing us with the data. VVA and AVS are grateful to the RFFI (Grant 96-02-17934) and INTAS-RFBR (Grant 95-0267) for financial support.

-
- [1] D. Alde et al., Zeit. Phys. **C66**, 375 (1995) ; A. A. Kondashov et al., in it Proc. 27th Intern. Conf. on High Energy Physics, Glasgow, 1994, p. 1407; Yu. D. Prokoshkin et al., Physics-Doklady **342**, 473 (1995); A. A. Kondashov et al, Preprint IHEP 95-137, Protvino, 1995.
- [2] F. Binon et al., Nuovo Cim. **A78**, 313 (1983).
- [3] F. Binon et al., Nuovo Cim. **A80**, 363 (1984).
- [4] V. V. Anisovich, A. A. Kondashov, Yu. D. Prokoshkin, S. A. Sadovsky, and A. V. Sarantsev, Phys. Lett. **B355**, 363 (1995).
- [5] V. V. Anisovich and A. V. Sarantsev, Phys. Lett. **B382**, 429 (1996).
- [6] V. V. Anisovich, Yu. D. Prokoshkin and A. V. Sarantsev, Phys. Lett. **B389**, 388 (1996).
- [7] S. J. Lindenbaum and R. S. Longacre, Phys. Lett. **B274**, 492 (1992); A. Etkin et al., Phys. Rev. D **25**, 1786 (1982).
- [8] V.V. Anisovich et al. Phys. Lett. **B323**, 233 (1994); C. Amsler et al., Phys. Lett. **B342**, 433 (1995); C. Amsler et al., Phys. Lett. **B355**, 425 (1995).
- [9] S. S. Gershtein, A. K. Likhoded, Yu. D. Prokoshkin, Zeit. Phys. **C24**, 305 (1984); C. Amsler and F. E. Close, Phys. Rev. D **53**, 295 (1996); Phys. Lett. **B353**, 385 (1995); V. V. Anisovich, Phys. Lett. **B364**, 195 (1995).
- [10] A. V. Anisovich, V. V. Anisovich, and A. V. Sarantsev, "Scalar glueball: Analysis of the $IJ^{PC} = 00^{++}$ -wave", hep-ph/9702339, Zeit. Phys. A, in press.
- [11] A. V. Anisovich and A. V. Sarantsev, "K-matrix analysis of the $K\pi$ S-wave in the mass region 900–2100 MeV and nonet classification of scalar $q\bar{q}$ states", hep-ph/9705401, Phys. Lett. B, in press.
- [12] G. t'Hooft, Nucl. Phys. **B72**, 161 (1974); G. Veneziano, Nucl. Phys. **B117**, 519 (1976).
- [13] V. V. Anisovich, M. G. Huber, M. N. Kobrinsky, and B. Ch. Metch, Phys. Rev. D **42**, 3045 (1990); K. Peters and E. Klempt, Phys. Lett. **B352**, 467 (1995); V. V. Anisovich, Phys. Lett. **B364**, 195 (1995); B. S. Zou, private communication.
- [14] V. V. Anisovich and V. M. Shekhter, Nucl. Phys. **B55**, 455 (1973); J. D. Bjorken and G. E. Farrar, Phys. Rev. D **9**, 1449 (1974).
- [15] M. A. Voloshin, Yu. P. Nikitin, and P. I. Porfirov, Sov. J. Nucl. Phys. **35**, 586 (1982).
- [16] G. S. Bali et al., Phys. Lett. **B309**, (1993) 378; J. Sexton, A. Vassarino and D. Weingarten, Phys. Rev. Lett. **75**, (1995) 4563; F. E. Close and M. J. Teper, "On the lightest glueball", preprint RAL-96-040, 1996; C. J. Morningstar and M. Peardon, "Efficient glueball simulations and anisotropic lattices", hep-lat/9704011 (1997).
- [17] A. V. Anisovich, V. V. Anisovich, Yu. D. Prokoshkin and A. V. Sarantsev, Zeit. Phys. **A357**, 123 (1997).
- [18] A. V. Anisovich, V. V. Anisovich and A. V. Sarantsev, Phys. Lett. **B395**, 123 (1997).
- [19] D. V. Bugg, V. V. Anisovich, A. V. Sarantsev and B. S. Zou, Phys. Rev. D **50**, 4412 (1994).
- [20] D. V. Bugg, A. V. Sarantsev and B. S. Zou, Nucl. Phys. **B471**, 59 (1996).
- [21] R. M. Barnett et al. (Particle Data Group), Phys. Rev. D **54**, 1 (1996).
- [22] D. Alde et al., Phys. Lett. **B241**, 600 (1990).
- [23] G. M. Beladidze et al., Zeit. Phys. **C54**, 367 (1992).
- [24] D. Aston et al., Nucl. Phys. **B296**, 493 (1988).
- [25] J. Weinstein and N. Isgur, Phys. Rev. D **27**, 588 (1983); *ibid* **D41**, 2236 (1990); D. Lohse et al., Nucl. Phys. **A516**, 513 (1996); G. Janssen et al., Phys. Rev. D **52**, 2690 (1995).
- [26] W. Flatté, Phys. Lett. **B63**, 224 (1976).

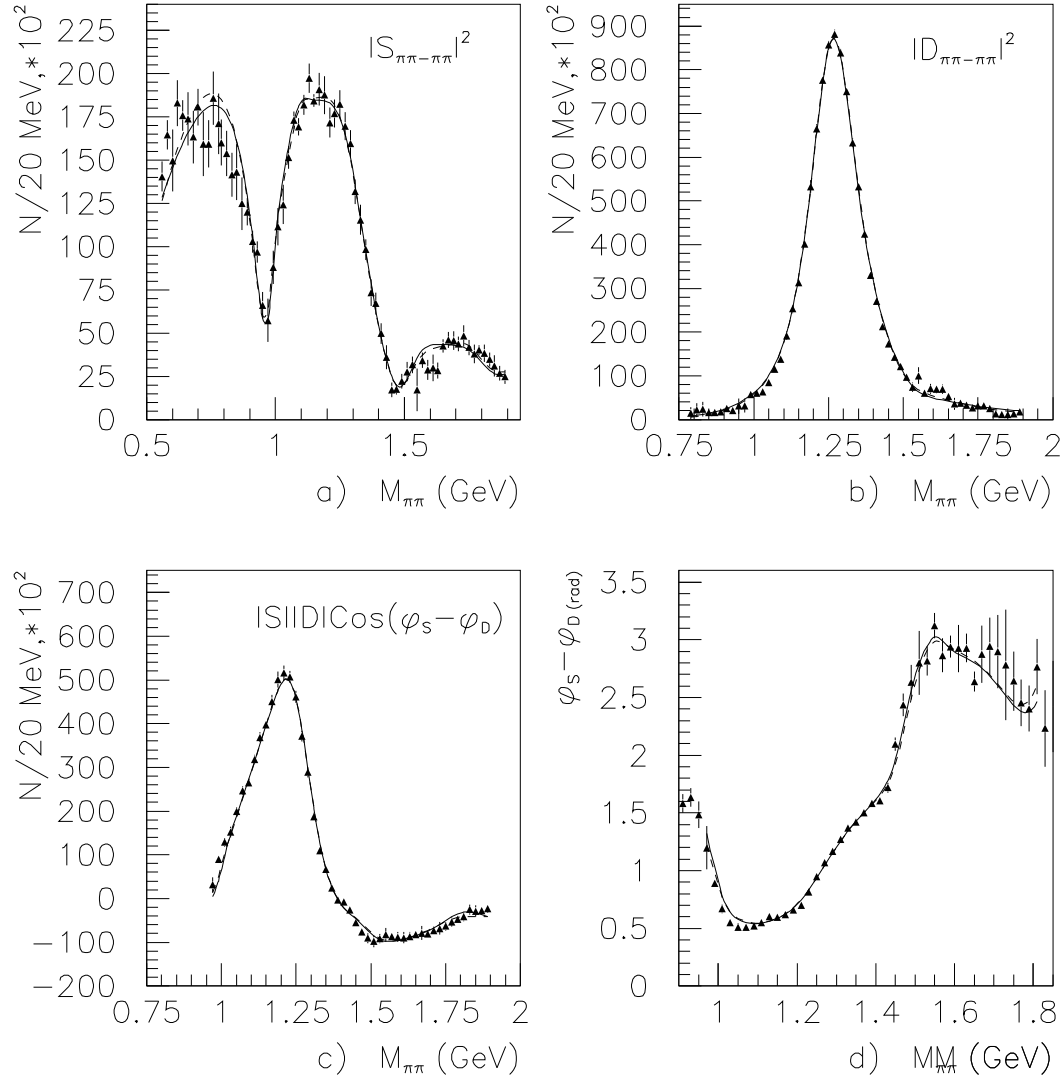


FIG. 2.

The $\pi\pi \rightarrow \pi\pi$ S -wave amplitude module squared [1] (a), the D -wave amplitude module squared (b), SD -correlator (c) and the phase difference between S and D -waves (d); the events are collected at the momentum transfer squared $|t| < 0.20 \text{ GeV}^2/c^2$ [1]. Solid curve corresponds to solution **II-2** and dashed one to solution **I**.

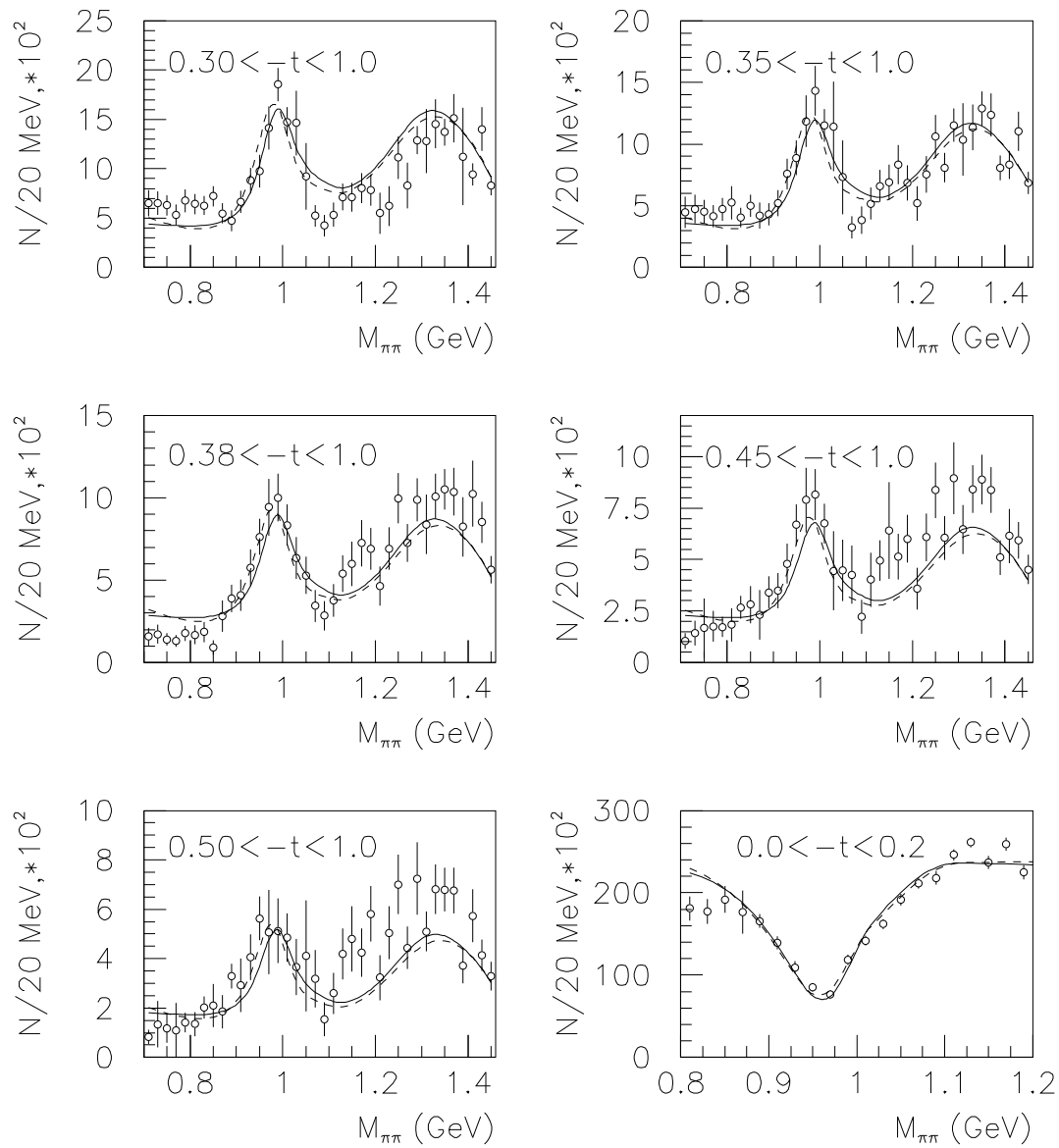


FIG. 3.

Event numbers *versus* invariant mass of the $\pi\pi$ -system in the S-wave for different t -intervals in the $\pi^-p \rightarrow \pi^0\pi^0n$ reaction [1]. Solid curves correspond to solution **II-2** and the dashed curves to solution **I**.

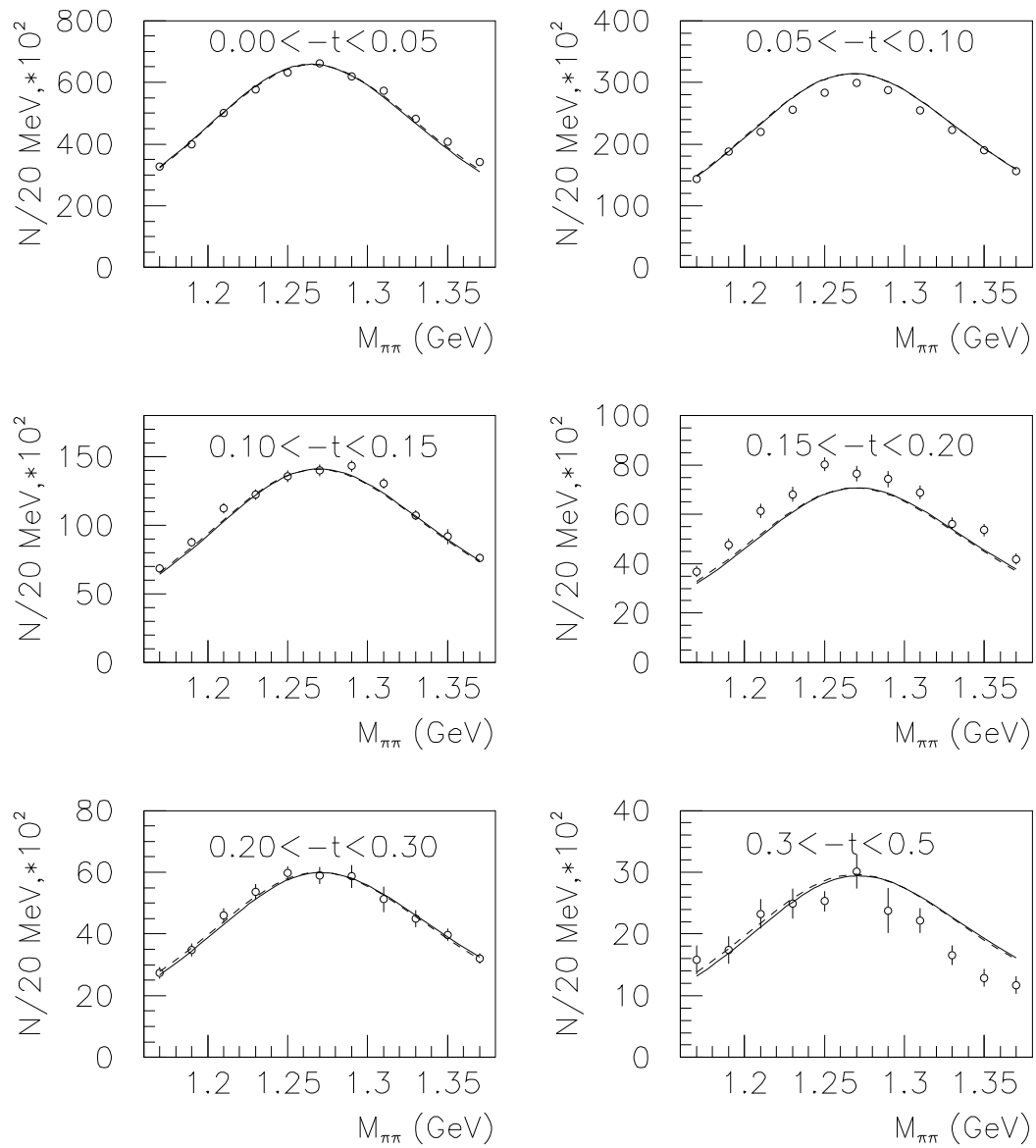


FIG. 4.

Event numbers *versus* invariant mass of the $\pi\pi$ -system in the D-wave for different t -intervals in the $\pi^- p \rightarrow \pi^0 \pi^0 n$ reaction [1]. The solid curves correspond to solution **II-2** and dashed one to solution **I**.

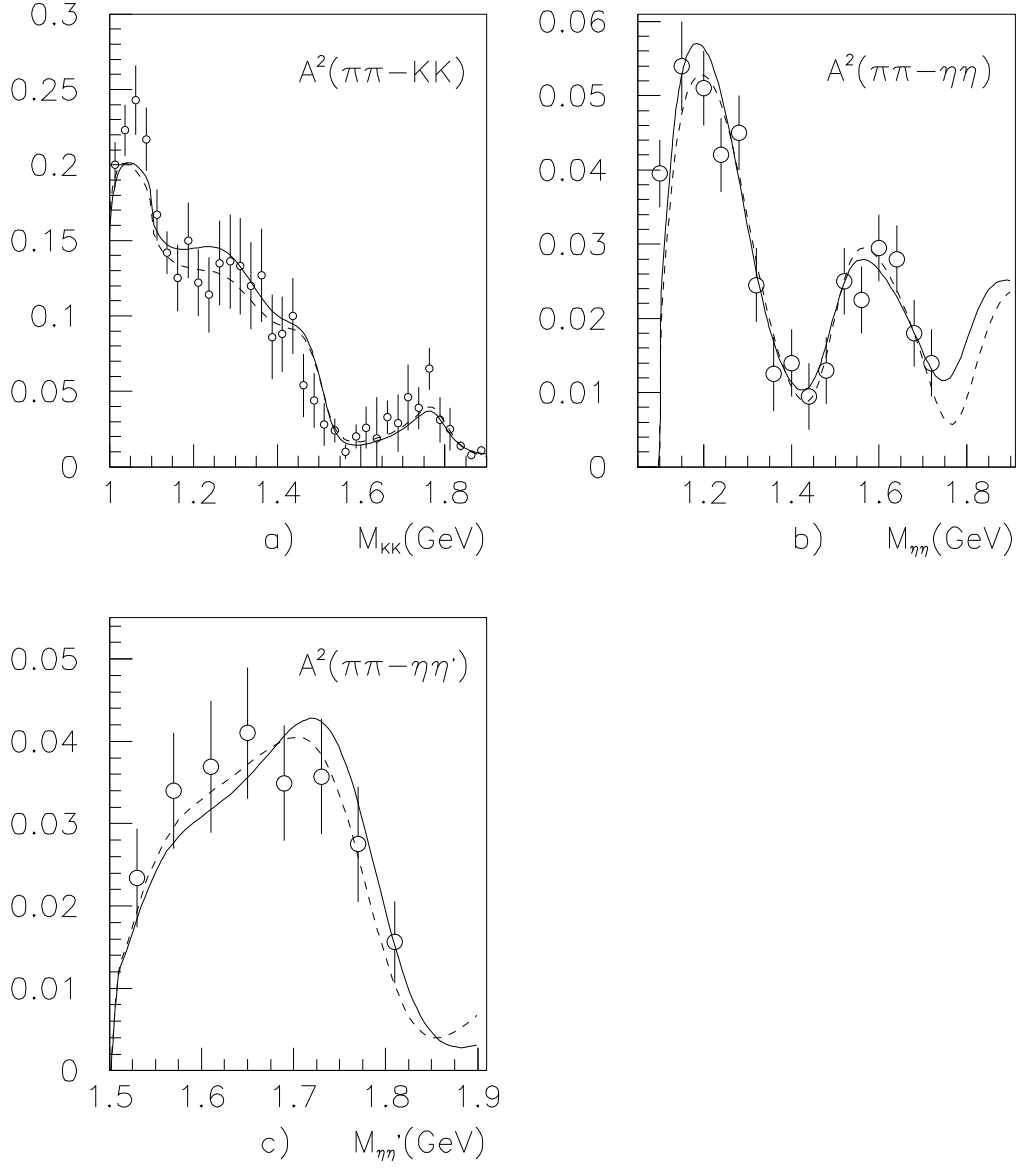


FIG. 5.

The S -wave amplitudes squared for transitions: (a) $\pi\pi \rightarrow K\bar{K}$ [7], (b) $\pi\pi \rightarrow \eta\eta$ [2] and (c) $\pi\pi \rightarrow \eta\eta'$ [3]. The solid curve corresponds to solution **II-2** and the dashed curve to solution **I**.

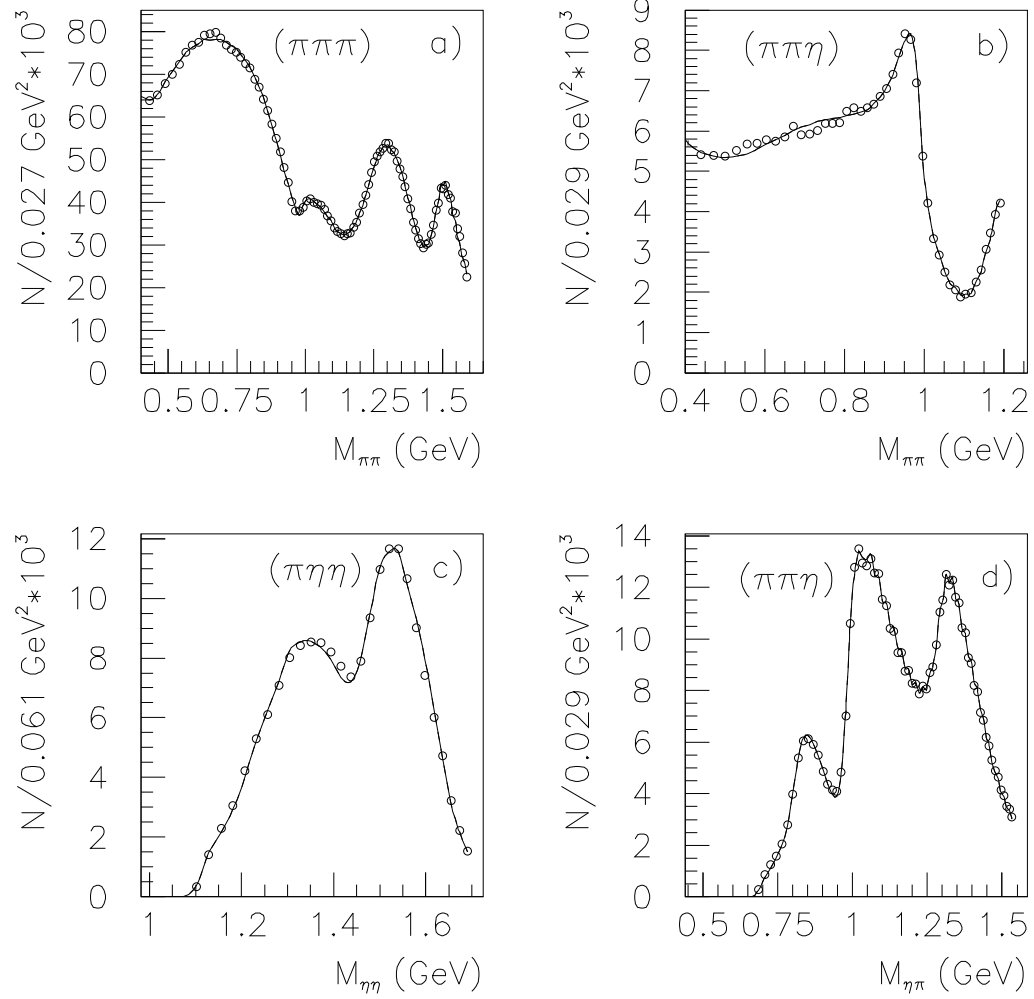


FIG. 6.

Mass projections of the Dalitz plot on the two-meson invariant mass for Crystal Barrel data. The curve corresponds to solution **II-2**.

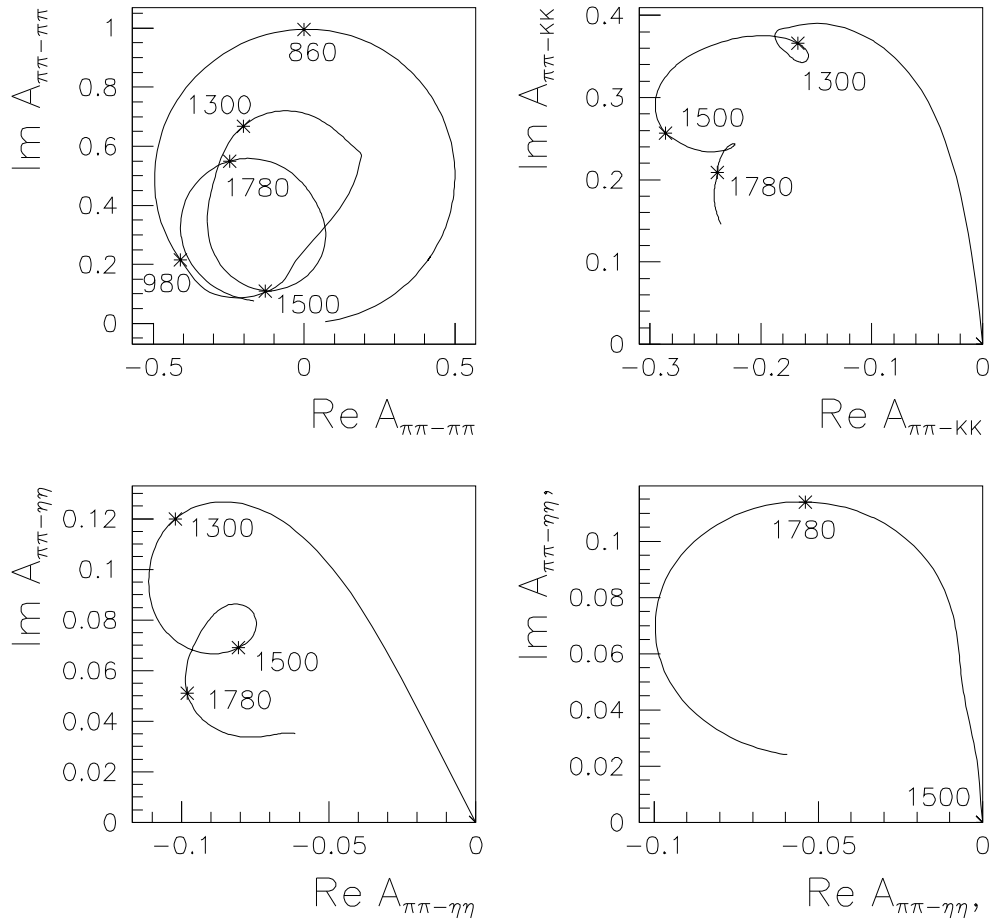


FIG. 7.

Argand plots for the S -wave scattering amplitudes in solution **II-2**: $\pi\pi \rightarrow \pi\pi$ (a), $\pi\pi \rightarrow K\bar{K}$ (b), $\pi\pi \rightarrow \eta\eta$ (c) and $\pi\pi \rightarrow \eta\eta'$ (d).

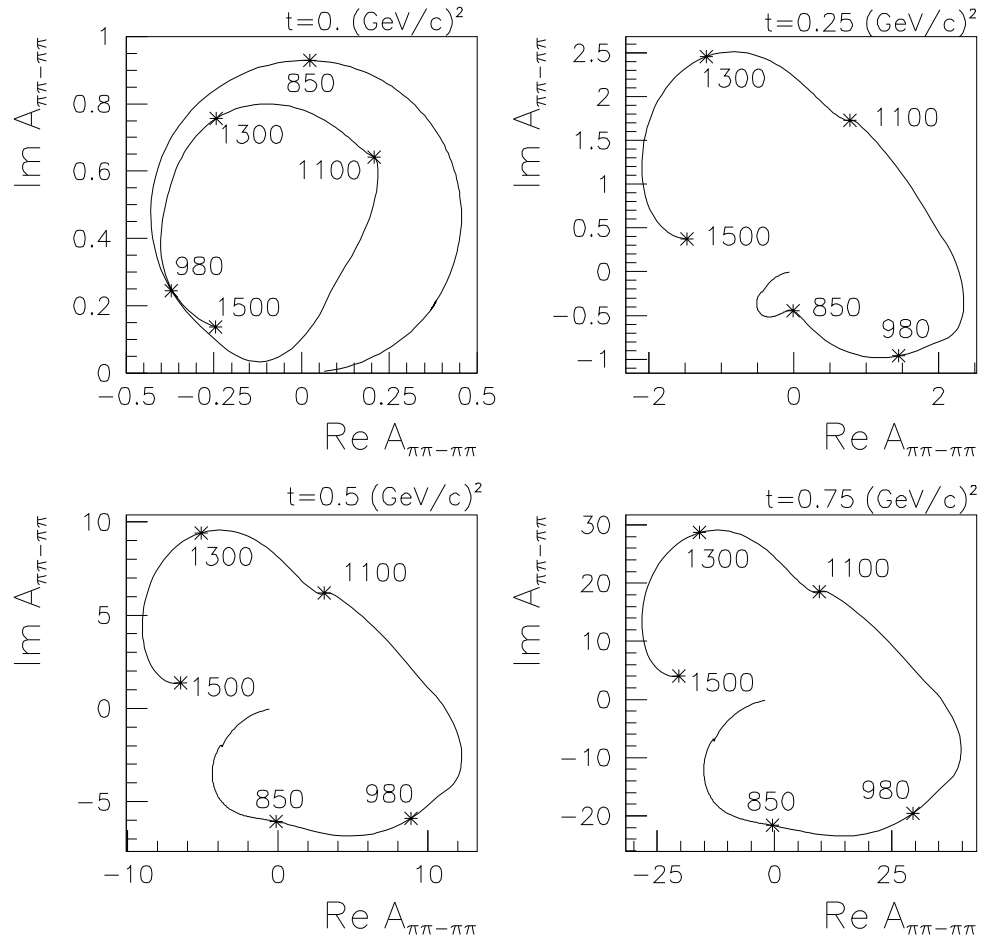


FIG. 8.
 Argand plots for the $\pi\pi(t) \rightarrow \pi\pi$ S-wave S-wave scattering amplitudes at different t .

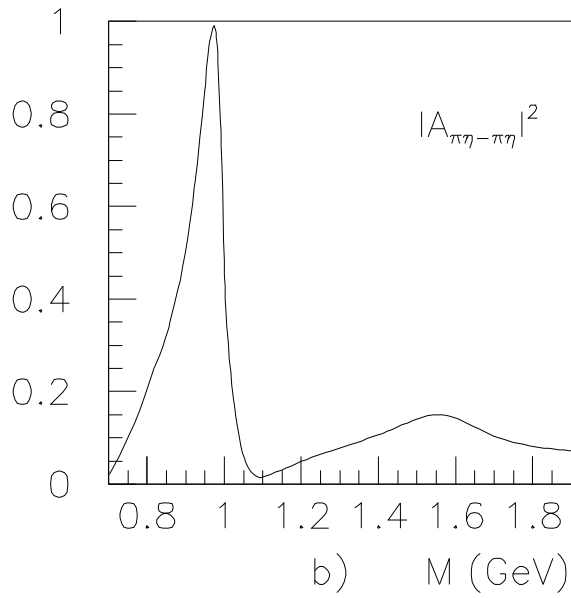
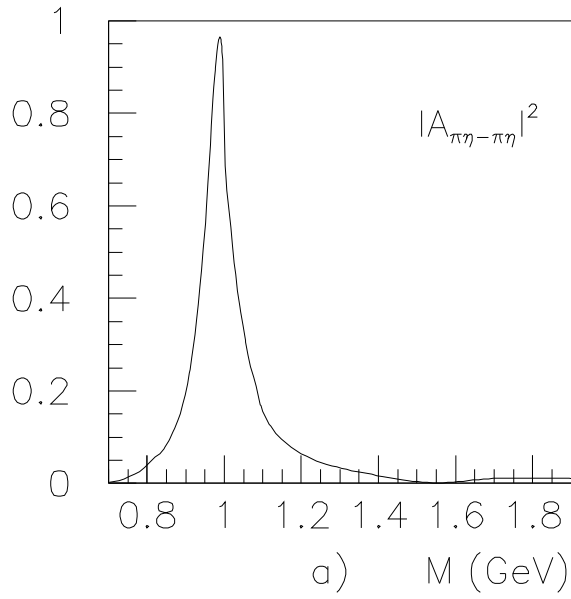


FIG. 9.

The squared S-wave $\pi\eta \rightarrow \pi\eta$ scattering amplitude: solutions 1 (a) and 2 (b) for the $\pi\eta \rightarrow \pi\eta$ scattering amplitude.

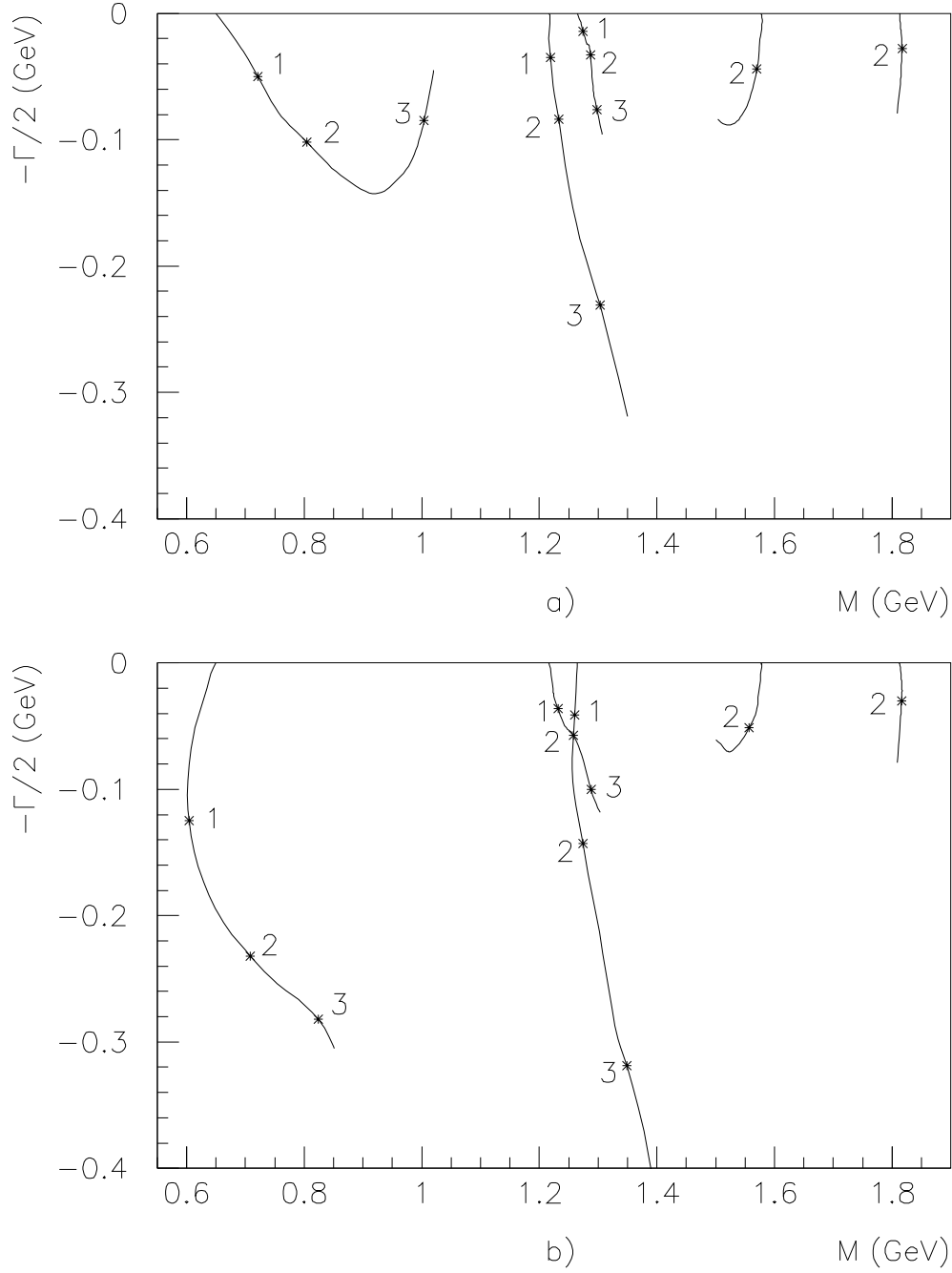


FIG. 10.

Location of 00^{++} amplitude poles in the complex- \sqrt{s} plane ($M = \text{Re}\sqrt{s}$, $-\Gamma/2 = \text{Im}\sqrt{s}$) after replacing $g_a^\alpha \rightarrow \xi g_a^\alpha$, on the sheet under the $\pi\pi$ cut (a) and on the sheet under $\pi\pi$ and $K\bar{K}$ cuts (b). The case $\xi \rightarrow 0$ gives the positions of masses of bare states; $\xi = 1$ corresponds to the real case. The point 1 corresponds to $\xi = 0.4$, 2 to $\xi = 0.6$ and 3 to $\xi = 0.9$.

TABLE I.

Coupling constants given by quark combinatorics for a $q\bar{q}$ -meson decaying into two pseudoscalar mesons in the leading terms of the $1/N$ expansion and for glueball decay in the next-to-leading terms of the $1/N$ expansion. Φ is the mixing angle for $n\bar{n}$ and $s\bar{s}$ states, and Θ is the mixing angle for $\eta - \eta'$ mesons: $\eta = n\bar{n}\cos\Theta - s\bar{s}\sin\Theta$ and $\eta' = n\bar{n}\sin\Theta + s\bar{s}\cos\Theta$. Glueball decay couplings in the leading terms of $1/N$ expansion are obtained by the replacements $g/\sqrt{2}\cos\Phi \rightarrow G^L$, $g\sin\Phi \rightarrow \sqrt{\lambda}G^L$.

Channel	The $q\bar{q}$ -meson decay couplings in the leading terms of $1/N$ expansion	Glueball decay couplings in the next-to-leading terms of $1/N$ expansion	Identity factor in phase space
$\pi^0\pi^0$	$g\cos\Phi/\sqrt{2}$	0	1/2
$\pi^+\pi^-$	$g\cos\Phi/\sqrt{2}$	0	1
K^+K^-	$g(\sqrt{2}\sin\Phi + \sqrt{\lambda}\cos\Phi)/\sqrt{8}$	0	1
K^0K^0	$g(\sqrt{2}\sin\Phi + \sqrt{\lambda}\cos\Phi)/\sqrt{8}$	0	1
$\eta\eta$	$g(\cos^2\Theta\cos\Phi/\sqrt{2} + \sqrt{\lambda}\sin\Phi\sin^2\Theta)$	$2g_G(\cos\Theta - \sqrt{\frac{\lambda}{2}}\sin\Theta)^2$	1/2
$\eta\eta'$	$g\sin\Theta\cos\Theta(\cos\Phi/\sqrt{2} - \sqrt{\lambda}\sin\Phi)$	$2g_G(\cos\Theta - \sqrt{\frac{\lambda}{2}}\sin\Theta)(\sin\Theta + \sqrt{\frac{\lambda}{2}}\cos\Theta)$	1
$\eta'\eta'$	$g(\sin^2\Theta\cos\Phi/\sqrt{2} + \sqrt{\lambda}\sin\Phi\cos^2\Theta)$	$2g_G(\sin\Theta + \sqrt{\frac{\lambda}{2}}\cos\Theta)^2$	1/2

TABLE II.

Coupling constants given by quark combinatorics for scalar mesons K_0^- and a_0^- decaying into two pseudoscalar mesons in the leading terms of the $1/N$ expansion.

Channel	The $s\bar{u}$ -meson decay couplings	Channel	The $d\bar{u}$ -meson decay couplings
$\bar{K}^0\pi^-$	$g(-)\frac{1}{2}$	$\eta\pi^-$	$g\frac{1}{\sqrt{2}}\cos\Theta$
$K^-\pi^0$	$g\frac{1}{\sqrt{8}}$	$\eta'\pi^-$	$g\frac{1}{\sqrt{2}}\sin\Theta$
$K^-\eta$	$g\frac{1}{\sqrt{8}}(\cos\Theta - \sqrt{2\lambda}\sin\Theta)$	K^0K^-	$g\frac{\sqrt{\lambda}}{2}$
$K^-\eta'$	$g\frac{1}{\sqrt{8}}(\sin\Theta + \sqrt{2\lambda}\cos\Theta)$	-	-

TABLE III.

 χ^2 values for the K-matrix solutions.

	Solution I	Solution II-1	solution II-2	Number of points
Crystal Barrel data [8]				
$p\bar{p} \rightarrow \pi^0 \pi^0 \pi^0$	1.52	1.41	1.42	1338
$p\bar{p} \rightarrow \pi^0 \eta \eta$	1.57	1.60	1.59	1798
$p\bar{p} \rightarrow \pi^0 \pi^0 \eta$	1.38	1.43	1.43	1738
$\pi^+ \pi^- \rightarrow \pi^0 \pi^0$				
S-wave GAMS data [1]	1.47	1.71	1.59	70
D-wave GAMS data [1]	1.63	2.16	2.14	56
SD-correlator [1]	1.82	2.26	2.12	47
t-dependent GAMS data [1]				
$0.00 < t < 0.20$	3.03	3.42	3.37	21
$0.30 < t < 1.00$	2.64	3.25	2.98	38
$0.35 < t < 1.00$	1.30	1.55	1.44	38
$0.40 < t < 1.00$	2.75	2.48	2.79	38
$0.45 < t < 1.00$	1.92	1.49	1.67	38
$0.50 < t < 1.00$	2.29	1.85	2.04	38
GAMS data [2,3]				
$\pi\pi \rightarrow \eta\eta$	0.70	0.97	0.87	16
$\pi\pi \rightarrow \eta\eta'$	0.49	0.65	0.64	8
$\pi\pi \rightarrow K\bar{K}$				
BNL data [7]	0.88	0.77	0.97	35

TABLE IV.

Masses, coupling constants (in GeV) and mixing angles (in degrees) for the f_0^{bare} -resonances for solution I. The errors reflect the boundaries for a satisfactory description of the data. II sheet is under the $\pi\pi$ and 4π cuts; IV sheet is under the $\pi\pi$, 4π , $K\bar{K}$ and $\eta\eta$ cuts; V sheet is under the $\pi\pi$, 4π , $K\bar{K}$, $\eta\eta$ and $\eta\eta'$ cuts.

	Solution I-1				
	$\alpha = 1$	$\alpha = 2$	$\alpha = 3$	$\alpha = 4$	$\alpha = 5$
M	$0.651^{+.120}_{-.030}$	$1.247^{+.150}_{-.030}$	$1.253^{+.015}_{-.045}$	$1.684^{+.010}_{-.045}$	$1.792^{+.040}_{-.040}$
$g^{(\alpha)}$	$1.318^{+.100}_{-.100}$	$0.597^{+.050}_{-.100}$	$0.879^{+.080}_{-.050}$	$0.702^{+.020}_{-.060}$	$0.702^{+.020}_{-.060}$
g_G	0	$-0.135^{+.050}_{-.050}$	0	0	0
$g_5^{(\alpha)}$	0	$0.944^{+.100}_{-.150}$	0	$0.898^{+.070}_{-.150}$	$0.302^{+.150}_{-.070}$
Φ_α	$-(71.5^{+3}_{-15})$	21.5^{+8}_{-8}	14.1^{+10}_{-5}	-6.0^{+10}_{-10}	89^{+5}_{-15}
	$a = \pi\pi$	$a = K\bar{K}$	$a = \eta\eta$	$a = \eta\eta'$	$a = 4\pi$
f_{1a}	$0.455^{+.100}_{-.100}$	$0.061^{+.100}_{-.100}$	$0.501^{+.100}_{-.100}$	$0.448^{+.100}_{-.100}$	$-0.129^{+.060}_{-.060}$
	$f_{ba} = 0$		$b = 2, 3, 4, 5$		
	$g_3^{(1)} = -0.259^{+.045}_{-.045}$		$g_4^{(1)} = -0.275^{+.010}_{-.010}$		$s_0 = 3.25^{+\infty}_{-1.0}$
II sheet	Pole position				
	$1.006^{+.008}_{-.008}$ $-i(0.048^{+.008}_{-.008})$				
IV sheet		$1.303^{+.010}_{-.020}$ $-i(0.138^{+.015}_{-.025})$	$1.496^{+.008}_{-.004}$ $-i(0.059^{+.005}_{-.005})$	$1.670^{+.100}_{-.150}$ $-i(0.760^{+.080}_{-.170})$	
V sheet					$1.775^{+.015}_{-.015}$ $-i(0.056^{+.015}_{-.010})$

TABLE V.

Masses, coupling constants (in GeV) and mixing angles (in degrees) for the f_0^{bare} -resonances for solutions II-1 and II-2.

	Solution II-1				
	$\alpha = 1$	$\alpha = 2$	$\alpha = 3$	$\alpha = 4$	$\alpha = 5$
M	$0.651^{+.120}_{-.030}$	$1.246^{+.150}_{-.035}$	$1.263^{+.015}_{-.045}$	$1.595^{+.030}_{-.040}$	$1.832^{+.030}_{-.050}$
$g^{(\alpha)}$	$1.385^{+.100}_{-.100}$	$0.375^{+.070}_{-.050}$	$0.923^{+.080}_{-.050}$	$0.424^{+.050}_{-.050}$	$0.424^{+.070}_{-.050}$
g_G	0	$-0.017^{+.050}_{-.050}$	0	0	0
$g_5^{(\alpha)}$	0	$0.705^{+.100}_{-.100}$	0	$0.552^{+.070}_{-.070}$	$-0.557^{+.070}_{-.070}$
Φ_α	$-(70.1^{+3}_{-15})$	30.0^{+8}_{-8}	18.3^{+8}_{-5}	20.6^{+08}_{-15}	-64.4^{+10}_{-10}
	$a = \pi\pi$	$a = K\bar{K}$	$a = \eta\eta$	$a = \eta\eta'$	$a = 4\pi$
f_{1a}	$0.440^{+.100}_{-.100}$	$-0.064^{+.100}_{-.100}$	$0.387^{+.100}_{-.100}$	$0.419^{+.100}_{-.100}$	$-0.165^{+.060}_{-.060}$
		$f_{ba} = 0$	$b = 2, 3, 4, 5$		
		$g_3^{(1)} = -0.239^{+0.045}_{-0.045}$	$g_4^{(1)} = -0.284^{+0.100}_{-0.100}$		$s_0 = 3.28^{+\infty}_{-1.0}$
II sheet	Pole position				
	$1.017^{+.008}_{-.008}$ $-i(0.049^{+.008}_{-.008})$				
IV sheet		$1.311^{+.010}_{-.020}$ $-i(0.117^{+.015}_{-.025})$	$1.500^{+.004}_{-.006}$ $-i(0.063^{+.003}_{-.006})$	$1.470^{+.150}_{-.100}$ $-i(0.545^{+.080}_{-.080})$	
V sheet					$1.814^{+.015}_{-.015}$ $-i(0.082^{+.025}_{-.010})$
	Solution II-2				
	$\alpha = 1$	$\alpha = 2$	$\alpha = 3$	$\alpha = 4$	$\alpha = 5$
M	$0.651^{+.120}_{-.030}$	$1.219^{+.150}_{-.030}$	$1.267^{+.015}_{-.045}$	$1.584^{+.010}_{-.045}$	$1.817^{+.040}_{-.040}$
$g^{(\alpha)}$	$1.351^{+.100}_{-.100}$	$0.435^{+.070}_{-.050}$	$0.901^{+.080}_{-.050}$	$0.433^{+.050}_{-.050}$	$0.435^{+.070}_{-.050}$
g_G	0	0	0	$-0.005^{+.050}_{-.050}$	0
$g_5^{(\alpha)}$	0	$0.719^{+.100}_{-.100}$	0	$0.542^{+.070}_{-.070}$	$-0.512^{+.070}_{-.070}$
Φ_α	$-(69.5^{+3}_{-15})$	40.7^{+8}_{-8}	19.6^{+10}_{-5}	20.0^{+08}_{-15}	-54^{+10}_{-10}
	$a = \pi\pi$	$a = K\bar{K}$	$a = \eta\eta$	$a = \eta\eta'$	$a = 4\pi$
f_{1a}	$0.459^{+.100}_{-.100}$	$0.046^{+.100}_{-.100}$	$0.405^{+.100}_{-.100}$	$0.420^{+.100}_{-.100}$	$-0.214^{+.060}_{-.060}$
		$f_{ba} = 0$	$b = 2, 3, 4, 5$		
		$g_3^{(1)} = -0.241^{+0.045}_{-0.045}$	$g_4^{(1)} = -0.273^{+0.100}_{-0.100}$		$s_0 = 3.05^{+\infty}_{-1.0}$
II sheet	Pole position				
	$1.020^{+.008}_{-.008}$ $-i(0.048^{+.008}_{-.008})$				
IV sheet		$1.304^{+.010}_{-.020}$ $-i(0.118^{+.015}_{-.025})$	$1.505^{+.004}_{-.008}$ $-i(0.063^{+.003}_{-.006})$	$1.420^{+.150}_{-.070}$ $-i(0.540^{+.080}_{-.080})$	
V sheet					$1.809^{+.015}_{-.015}$ $-i(0.080^{+.025}_{-.010})$

TABLE VI.

Masses and coupling constants (in GeV) for a_0 resonances. The star denotes that the parameter is fixed.

a_0 -resonances without K-matrix background term				
	Solution I-1		Solutions II-(1,2)	
	$\alpha = 1$	$\alpha = 2$	$\alpha = 1$	$\alpha = 2$
M	$0.963^{+.015}_{-.015}$	$1.630^{+.100}_{-.040}$	$0.965^{+.015}_{-.015}$	$1.654^{+.100}_{-.040}$
$g^{(\alpha)}$	$0.879^{+.100}_{-.100}$	0.702*	$0.901^{+.100}_{-.100}$	0.435*
$g_4^{(\alpha)}$	$0.598^{+.150}_{-.050}$	$0.511^{+.060}_{-.060}$	$0.689^{+.150}_{-.050}$	$0.687^{+.080}_{-.080}$
Pole position				
II sheet	$0.987^{+.005}_{-.005}$ $-i(0.045^{+.005}_{-.005})$		$0.989^{+.005}_{-.005}$ $-i(0.048^{+.010}_{-.010})$	
III sheet	$0.964^{+.015}_{-.015}$ $-i(0.070^{+.010}_{-.010})$		$0.965^{+.015}_{-.015}$ $-i(0.073^{+.010}_{-.010})$	
	$1.558^{+.025}_{-.025}$ $-i(0.141^{+.015}_{-.015})$		$1.571^{+.025}_{-.025}$ $-i(0.151^{+.015}_{-.015})$	
a_0 -resonances with K-matrix background term				
	Solution I-1		Solutions II-(1,2)	
	$\alpha = 1$	$\alpha = 2$	$\alpha = 1$	$\alpha = 2$
M	$0.944^{+.015}_{-.015}$	$1.624^{+.100}_{-.030}$	$0.939^{+.015}_{-.015}$	$1.640^{+.100}_{-.040}$
$g^{(\alpha)}$	$0.879^{+.100}_{-.100}$	0.702*	$0.901^{+.100}_{-.100}$	0.435*
$g_4^{(\alpha)}$	$0.651^{+.100}_{-.080}$	$0.519^{+.060}_{-.060}$	$0.653^{+.150}_{-.050}$	$0.651^{+.080}_{-.080}$
	$f_{11} = 0.529^{+.100}_{-.100}$	$s_0 = 1.0^{+2.0}_{0.3}$	$f_{11} = 0.731^{+.100}_{-.100}$	$s_0 = 1.9^{+2.0}_{0.8}$
Pole position				
II sheet	$0.990^{+.005}_{-.005}$ $-i(0.039^{+.005}_{-.005})$		$0.993^{+.005}_{-.005}$ $-i(0.042^{+.010}_{-.010})$	
III sheet	$0.965^{+.015}_{-.015}$ $-i(0.063^{+.010}_{-.010})$		$0.965^{+.015}_{-.015}$ $-i(0.068^{+.010}_{-.010})$	
	$1.559^{+.025}_{-.025}$ $-i(0.145^{+.015}_{-.015})$		$1.575^{+.025}_{-.025}$ $-i(0.153^{+.015}_{-.015})$	

TABLE VII.

Masses and coupling constants (in GeV) for f_2 and a_2 resonances.

f_2 -resonances				
Solution I-1		Solutions II-(1,2)		
	$\alpha = 1$	$\alpha = 2$	$\alpha = 1$	$\alpha = 2$
M	$1.236^{+.010}_{-.010}$	$1.530^{+.010}_{-.010}$	$1.233^{+.010}_{-.005}$	$1.529^{+.010}_{-.010}$
$g^{(\alpha)}$	$1.342^{+.100}_{-.100}$	$1.342^{+.100}_{-.100}$	$1.038^{+.100}_{-.100}$	$1.038^{+.100}_{-.100}$
Φ_α	$-(8.4^{+2.0}_{-3.0})$	$86.6^{+2.5}_{-4.5}$	$-(8.8^{+2.0}_{-3.0})$	$86.2^{+2.5}_{-4.5}$
$g_{4\pi}^{(\alpha)}$	$0.318^{+.020}_{-.020}$	$0.448^{+.020}_{-.020}$	$0.318^{+.020}_{-.020}$	$0.472^{+.020}_{-.020}$
	$a = \pi\pi$	$a = \eta\eta$	$a = \pi\pi$	$a = \eta\eta$
f_{1a}	$0.742^{+.050}_{-.250}$	$-(1.01^{+.050}_{-.500})$	$0.287^{+.070}_{-.070}$	$-0.143^{+.100}_{-.100}$
r_a	$1.997^{+.150}_{-.150}$	$1.077^{+.050}_{-.500}$	$2.474^{+.150}_{-.150}$	$1.295^{+.150}_{-.150}$
	$f_{13} = 0.684 \pm 0.100$	$f_{ba} = 0, b = 2, 3, s_0 = 5.0$	$f_{13} = 0.578 \pm 0.100$	
Pole position	$1.262^{+.005}_{-.005}$ $-i(0.092^{+.005}_{-.005})$	$1.514^{+.010}_{-.006}$ $-i(0.066^{+.008}_{-.005})$	$1.261^{+.005}_{-.005}$ $-i(0.089^{+.005}_{-.005})$	$1.522^{+.005}_{-.010}$ $-i(0.076^{+.005}_{-.007})$
a_2 -resonances				
Solution I-1		Solutions II-(1,2)		
	$\alpha = 1$	$\alpha = 2$	$\alpha = 1$	$\alpha = 2$
M	$1.316^{+.005}_{-.005}$	$1.645^{+.050}_{-.050}$	$1.312^{+.005}_{-.005}$	$1.695^{+.050}_{-.080}$
$g^{(\alpha)}$	$1.080^{+.100}_{-.100}$	$0.270^{+.100}_{-.100}$	$1.300^{+.100}_{-.100}$	$0.325^{+.100}_{-.100}$
$g_4^{(\alpha)}$	$0.381^{+.050}_{-.050}$	$0.597^{+.050}_{-.050}$	$0.426^{+.050}_{-.050}$	$0.617^{+.050}_{-.050}$
	$r_1 = 1.845^{+.150}_{-.150}$		$r_1 = 2.406^{+.150}_{-.150}$	
Pole position	$1.309^{+.005}_{-.005}$ $-i(0.058^{+.005}_{-.005})$	$1.615^{+.030}_{-.030}$ $-i(0.121^{+.015}_{-.015})$	$1.308^{+.005}_{-.005}$ $-i(0.059^{+.005}_{-.005})$	$1.667^{+.030}_{-.030}$ $-i(0.123^{+.015}_{-.015})$